

Physical and microstructural impacts on the hydro-mechanical behaviour of Ypresian clays

X.P. Nguyen, Yu-Jun Cui, Anh Minh A.M. Tang, X.L. Li, L. Wouters

▶ **To cite this version:**

X.P. Nguyen, Yu-Jun Cui, Anh Minh A.M. Tang, X.L. Li, L. Wouters. Physical and microstructural impacts on the hydro-mechanical behaviour of Ypresian clays. Applied Clay Science, 2014, 102, pp.172-185. 10.1016/j.clay.2014.09.038 . hal-01119445

HAL Id: hal-01119445

https://enpc.hal.science/hal-01119445

Submitted on 23 Feb 2015

HAL is a multi-disciplinary open access archive for the deposit and dissemination of scientific research documents, whether they are published or not. The documents may come from teaching and research institutions in France or abroad, or from public or private research centers.

L'archive ouverte pluridisciplinaire **HAL**, est destinée au dépôt et à la diffusion de documents scientifiques de niveau recherche, publiés ou non, émanant des établissements d'enseignement et de recherche français ou étrangers, des laboratoires publics ou privés.

Physical and microstructural impact on the hydro-mechanical behaviour of Ypresian clays

X. P. Nguyen[1,*], Y. J. Cui[1], A. M. Tang[1], X. L. Li[2], L. Wouters[3]

1. Laboratoire Navier (UMR 8205), CNRS, ENPC, IFSTTAR, Université Paris-Est, F-77455 Marne-la-Vallée, France (phunguyenx@gmail.com; yujun.cui@enpc.fr; anhminh.tang@enpc.fr)
2. ESV EURIDICE GIE, Boeretang 200, BE-2400, MOL, Belgium (xli@euridice.be)
3. ONDRAF/NIRAS, Avenue des Arts, BE-1210, Brussels, Belgium (l.wouters@nirond.be)

*. Presently at CEA, DEN, DPC, SECR, Laboratoire d'Étude du Comportement des Bétons et des Argiles, F-91191 Gif-sur-Yvette, France

Corresponding author:

Dr Xuan Phu NGUYEN
CEA, DEN, DPC, SECR, LECBA
Bat. 133, P. 103F
F-91191 Gif-sur-Yvette
France
Telephone: +33 1 69 08 33 48
Email: phunguyenx@gmail.com

Abstract: An experimental characterisation on Ypresian clays that are considered as one of the potential geological host formations for the radioactive waste disposal in Belgium has been carried out. Physical, microstructural, hydraulic and mechanical properties were investigated on the samples taken from a cored borehole at Kallo in the Northern Belgium at 290 - 400 m depth. Identification tests, scanning electron microscopy (SEM), mercury intrusion porosimetry (MIP) and œdometer tests were performed. The results obtained showed that Ypresian clays are highly plastic and their physical and mineralogical properties present significant variations over depth. Compared to Boom Clay, the other potential host formation for the radioactive waste disposal in Belgium, Ypresian clays show (i) clearly higher liquid limit and specific surface, especially for its basal part ; (ii) lower density despite its deeper location; and (iii) lower degree of saturation of samples. These features were related to a bi-modal pore-size distribution which is quite particular for a sediment at such depth. Furthermore, it has been observed that the compressibility and swelling capacity of Ypresian clays increase with depth while the permeability decreases despite the increase in void ratio. The normalized compression curves confirm the soil compressibility variations over depth and the slightly over-consolidated state of Ypresian clays.

Keywords: Ypresian clays; physical properties; microstructure; hydro-mechanical behaviour.

1. Introduction

Ypresian clays, situated between 290 - 400 m depth at Kallo (Northern Belgium), are considered as a potential host formation in the Belgian high-level and/or long-lived (HL/LL) radioactive waste disposal program. As opposed to the situation of Boom Clay, another potential host formation which has been extensively investigated since the seventies in the laboratory and also *in situ* in the "High Activity Disposal Experimental Site" Underground Research Laboratory (HADES URL), the characterisation of Ypresian clays has been quite limited: before 1997, geotechnical data on Ypresian clays were scarce and scattered as only few boreholes reaching the bottom of the formation had been drilled by the Geological Survey of Belgium and other bodies for different purposes. The first investigation campaign on Ypresian clays in the framework of the research & development programme of radioactive waste disposal was started in 1997 - 1998 with several cored boreholes at the Doel site, situated in the North of the Antwerp city. This campaign focused on the mineralogy, geochemistry, hydrology and physical properties (Van Marcke and Laenen, 2005). Several boreholes were drilled at Kallo in 2008 - 2009 (Cammaer et al., 2009), about 10 km to the south of Doel, enabling the geomechanical characterisation of the Ypresian clays.

In the present work, four cores of Ypresian clays taken at different depths from the ON-Kallo-1 borehole were characterised in terms of physical properties, microstructure features, hydraulic and mechanical behaviours. Moreover, by analysing and integrating the data of Ypresian clays gathered at Doel (see Van Marcke and Laenen, 2005), a complete description of the variations of Ypresian clays' physical and microstructural properties in the horizontal and vertical directions is given, the impact of these variations on the hydro-mechanical behaviour was also analysed.

2. Materials and experimental methods

2.1. Geological description

The Ieper Group was deposited during the Ypresian period (55 - 49.6 million years ago) in the northwestern half of Belgium. It outcrops in the southern part of the depositional area, gently dips and thickens toward the Northeast (Figure 1). The group comprises three marine sediment formations, Kortrijk, Tielt and Gent, and corresponds roughly to London clay in Southeast London, the “argile des Flandres” and the “argile Plastique” in Northern France (Van Marcke and Laenen, 2005).

The term “Ypresian clays” refers to the sediments deposited during Early and Middle Ypresian times including the Kortrijk Formation (Members of Orchies, Roubaix and Aalbeke) and a part of the overlying Tielt Formation (Kortemark Member; Figure 2). At the Kallo site, Ypresian clays were found between 289 and 400 m below surface: the Kortemark Member between 289 - 303 m depth, Aalbeke Member 303 - 311 m, Roubaix Member 311 - 380 m and between 380 - 400 m depth the Orchies Member.

As Ypresian clays were deposited in a neritic environment in the southern border of the North Sea, their properties are significantly influenced by the transgressive - regressive cycles during their sedimentation: (i) the grading trend is fining-upward for transgression while coarsening-upward for regression; and (ii) the clay-size mineralogy is composed of more kaolinite, illite and chlorite (non-expansive clay minerals) for transgression due to a distant detrital population source, but higher smectite for regression (Van Marcke and Laenen, 2005). The main transgressive - regressive cycles corresponding to the Ypresian clays’ sedimentology at Kallo were estimated as shown in Figure 2 (Cammaer et al., 2009; Van Marcke and Laenen, 2005). Note that these main cycles can be further divided into several sub-cycles of higher resolution.

94 The burial history of Ypresian clays at Doel shows several deposition - erosion cycles, resulting
95 in a c.a. 50 m difference between the present depth and the maximum one in the history (Van
96 Marcke and Laenen, 2005). Considering the vicinity between the Doel site and the Kallo site, we
97 can consider that the two sites have a similar degree of over-consolidation.

98 It is noteworthy to distinguish the yield stress σ'_y from the pre-consolidation stress σ'_p (and thus,
99 correspondingly, the yield stress ratio $YSR = \sigma'_y/\sigma'_{v0}$ from the over-consolidation one $OCR =$
100 σ'_p/σ'_{v0}): (i) the latter results solely from mechanical unloadings, such as erosion or arising of
101 water table (geological over-consolidation). It is estimated based on the maximal burial depth in
102 the geological history; while (ii) the former involves, in addition, others geological phenomena,
103 for example creep, digenesis, weathering, cambering and valley bulging…. It can be determined
104 from œdometer test in the laboratory (Burland, 1990; Chandler, 2000). Naturally, $\sigma'_y \geq \sigma'_p$ and
105 $YSR \geq OCR$ (see Figure 16).

106 *2.2. Physical properties*

107 The four soil cores investigated in this study are from the borehole ON-Kallo-1 drilled by
108 ONDRAF/NIRAS in 2008 - 2009 (Cammaer et al., 2009), and they are indicated in Figure 2:
109 YK43 and YK64 are in the middle of the Roubaix Member, YK73 is in the lower part of the
110 Roubaix Member and YK95 is taken in the upper part of the Orchies Member. Note that the soil
111 cores were named by the initials of the formation and the site followed by its number in the
112 borehole. For instance, YK43 means core number 43 of Ypresian clays from the borehole at
113 Kallo. These cores were contained in PVC tubes of 96 mm in inner diameter and of 1 m in
114 length, and wrapped in vacuumed aluminium foil. The two ends of each PVC tube were not

sealed by wax; thus water loss would occur by evaporation before laboratory testing (2010 - 2011).

Figure 3 shows the particle-size distribution curves of the four adjacent cores (YK44, 63, 74 and 96) by laser technique (Vandenberghe, 2011). It appears that the clay-size (< 2 µm) fractions of all cores are higher than 55 %. The Roubaix Member is known to be siltier (coarser) than the Orchies (YK96) and Aalbeke Members, and this is clearly reflected in the granulometer curves. The three Roubaix Member samples have a relatively similar granulometer distribution. It should be noted that for a given soil, significant difference may exist between particle-size distribution curves obtained by laser technique and by sieving and hydrometer, particularly for clayey soils (Nguyen, 2013).

The mineralogical composition of the four previously mentionned cores by X-ray diffractometry and cation exchange capacity (CEC) measurement (Co-hexamine technique) is presented in Table 1 for the bulk mass and in

Table 2 for the clay-size fraction (Vandenberghe, 2011). It appears that the non-clay minerals represent less than half in bulk mass, and the clay minerals are dominated by expansive ones (smectite and interstratified illite - smectite) that represent more than 80 % in clay-size (> 2 µm) fraction and about two thirds in bulk mass. Moreover, the total clay minerals and the expansive ones are quite similar for these four cores.

The physical and index properties of YK 43, 64, 73 and 95 are presented in Table 3. The values of Atterberg's limits of the Kallo samples (this study) together with those of Doel (Van Marcke and Laenen, 2005) were used for establishing the classification of the Ypresian clays according to ASTM (2006) (see Figure 4). It can be observed that the Ypresian clays are highly plastic at

both the Kallo site and the Doel site. In particular, a liquid limit higher than 130 is identified on YK73 and YK95. A large variability over depth of soils is also observed for both sites: YK73 (lower part of the Roubaix Member) and YK95 (upper part of the Orchies Member) have clearly higher values of liquid limit and plasticity index than YK43 and YK64 (middle part of the Roubaix Member). This is in agreement with the blue methylene value (*VBS*) determined according to AFNOR (1998) and the specific surface S_s deduced from *VBS* (Tran, 1980). A clear distinction between these two groups of samples, (YK43, 64) and (YK73, 95), can also be observed through other parameters presented in Table 3 such as unit mass ρ_0, dry unit mass ρ_{d0}, void ratio e_0, porosity n_0 and water content w_0: the two upper cores (YK43, 64) show higher ρ_0 and ρ_{d0} (lower e_0, n_0 and w_0) than the two lower ones (YK73, 95). The carbonate contents of Ypresian clays are low, except for YK43 that has a particularly high value of 10.2 g/100g. The degree of saturation S_{r0} is lower than 100% for all samples, mainly owing to the water loss during the sample conservation as stated above.

2.3. Microstructural properties

Figure 5 shows the Scanning Electron Microscope (SEM) photos of YK 43, 64, 73 and 95 on the section perpendicular to the bedding plane. A dominance of silt grains with size up to 10 µm are identified for the two upper cores, especially for YK43. On the contrary, for the two lower cores, a clay particle matrix is observed with dispersed silt grains. This is more or less consistent with the grain-size distribution curves as shown in Figure 3: the fraction of particles larger than 10 µm in (YK44, 63) is about 20 %, against only 15 % and 5 % in YK74 and YK96, respectively. However, the important difference between YK74 and YK96 in grain-size distribution is not observed in this SEM results.

159 Figure 6 shows the pore-size distribution (PSD) curves of YK43, 73 and 95 by mercury intrusion
160 porosimetry (MIP) in terms of intruded mercury void ratio e_m, defined as the ratio of mercury
161 intrusion volume V_m to soil solid volume V_s, versus the entrance diameter D as well as $\delta e_m/\delta \log D$
162 versus log$D$. It should be noted that the MIP technique used can only cover a range of pore sizes
163 from D = 300 to 0.005 µm, corresponding to a range of injection pressure from 0.1 to 200 MPa,
164 and that the MIP tests on YK95 and YK43 were prematurely stopped due to a technical problem.
165 It is observed that YK73 (lower part of the Roubaix Member) and perhaps YK95 (upper part of
166 the Orchies Member) present bi-modal porosity with the density of the micro-pore family (D =
167 0.06 µm for YK73) clearly higher than that of the second family (D = 0.25 µm). The pore-size
168 family around D = 100 µm can be explained by the technical perturbation during the preparation
169 of samples. By contrast, YK43 (middle part of the Roubaix Member) shows a mono-modal
170 porosity with a sole dominant pore family of D = 0.8 µm. A macro-pore family at D = 5 µm is
171 identified for YK43 but its density is negligible. This mono-modal porosity is typical for deep
172 sediments such as Boom Clay at Mol (Coll, 2005; Dehandschutter et al., 2004; Lima, 2011) and
173 at Essen (Nguyen, 2013).

174 *2.4. Experimental methods for investigating the hydro-mechanical behaviour*

175 Both high- and low-pressure œdometers (HPO and LPO) were used. The LPO had only one lever
176 arm multiplying the load by 10 on the sample, allowing applying a vertical stress σ_v up to 3.2
177 MPa on a sample of 50 mm diameter. The HPO had a double lever arm with one lever arm
178 multiplying the load by 5 and the other by 10, allowing applying a vertical stress σ_v up to 64
179 MPa on a sample of 50 mm diameter.

The soil samples were hand-trimmed to reach the dimensions of 50 mm in diameter and 20 mm in height. The initial states of the tested samples are shown in Table 4 with soil initial water content w_0, void ratio e_0, porosity n_0, degree of saturation S_{r0} and density ρ_0 as well as the void ratio under the *in situ* vertical effective stress, $e_{\sigma'v0}$. The HPO tests are numbered 1 while the LPO tests are numbered 2. In order to account for the deformability of the loading system in the HPO tests, calibration was carried out without sample in the œdometer cell following the same loading path as shown in Figure 7.

Typical test procedures for HPO and LPO tests are presented in Figure 7 and Figure 8, respectively. After installing the soil sample in the œdometer cell, step loading (A - B) up to the *in situ* vertical effective stress σ'_{v0}, rounded for practical convenience to 3.2 MPa, was undertaken without putting the sample in contact with water in order to avoid soil swelling which would modify the soil microstructure (AFNOR, 1997; Delage et al., 2007; Deng et al., 2011a, 2011b, 2011c, 2012). Afterwards, the bottom porous stone and the drainage system were then filled with synthetic Ypresian clays water (SYCW) consisting of 8.896 g NaCl and 0.896 g Na_2SO_4 in 1 L solution (Van Marcke, 2009). For HPO tests, two stepwise unloading - reloading loops between $\sigma_v = \sigma'_{v0}$ (C) - 0.2 (D) - 16 (E) - 0.2 (F) - 32 (G) MPa and a final unloading from σ_v = 32 MPa (G) to 0.2 MPa (H) were then undertaken (Figure 7). For LPO tests, unloading from σ'_{v0} to 0.05 MPa (C-D), reloading from 0.05 MPa to 3.2 MPa (D-E) and unloading again to 0.05 MPa (E-F) were conducted (Figure 8). The French standard (AFNOR, 1997) was applied for the volume change criterion: the volume change was considered as steady when the vertical strain rate was lower than 5×10^{-4}/8 h.

3. Experimental results

3.1. Compressibility and swelling capacity

Low- and high-pressure œdometer compression curves of YK43, 64, 73 and 95 are presented in Figure 9, 10, 11 and 12, respectively. The values of degree of saturation S_r during the initial loading (AB), before soaking (putting in contact with SYCW), were determined by assuming a constant water content $w = w_0$ and indicated on the curves. It appears that all soil samples reached full saturation at the end of this process, under $\sigma_v = \sigma'_{v0}$ = 3.2 MPa, except the YK64O1 sample with a final value of 98 % (Figure 10b). As all the curves are clearly non-linear, the compression index C^*_c and swelling index C^*_s are adopted that correspond respectively to the slopes of each (re)loading and unloading (Deng et al., 2011a). An increase of C^*_c when S_r approaches 100 % is observed, especially for YK73 and 95. Le et al. (2011) conducted œdometer tests on unsaturated Boom Clay samples with suction measurement and observed that this increase in C^*_c corresponds to the suction becoming zero when pore water started to be squeezed out.

Upon soaking, slight compressions are observed for all the tests. For YK64, 73 and 95, the void ratios $e_{\sigma'v0}$ under the *in situ* vertical effective stress $\sigma_v = \sigma'_{v0}$ = 3.2 MPa (point C) in LPO and HPO tests are almost the same (Table 4). On the contrary, for YK43, the value of $e_{\sigma'v0}$ in LPO test (0.64) is smaller than that in HPO test (0.70). Note that the YK43 sample in LPO test has a smaller initial void ratio e_0 than that in HPO test (0.78 against 0.81), but this difference is smaller than that under the *in situ* stress (0.03 against 0.06).

Upon the first unloading after soaking (C-D), two swelling fashions are identified: for YK43 and 64, the void ratio at the end of this unloading, under σ_v = 0.21 MPa in HPO test and 0.05 MPa in LPO test (point D), is smaller than its initial value e_0, while for YK73 and 95 the inverse is

observed, showing a higher swelling capacity than the two samples taken at upper depths. Note that the densities of YK73 and 95 samples at the beginning of this unloading under σ_v = 3.2 MPa (point C) are lower than those of YK43 and 64 samples (see Table 4).

For all the four samples at different depths, the compression curves upon this unloading (C-D) are clearly non-linear as the swelling index C^*_s increases with the decrease of vertical stress σ_v. A roughly bi-linear shape was adopted by Cui et al. (2013) with a small slope C_{se1} that corresponds to a mechanical rebounding under high vertical stress and a larger slope C_{sp1} that corresponds to a physico-chemical swelling under lower vertical stress, the two parts being separated by a swelling stress σ_{s1} (Figure 13).

During the first reloading (D-E), the non-linearity of the curve was considered by Cui et al. (2013) as tri-linear: (i) when $\sigma_v < \sigma'_{v0}$ = 3.2 MPa, the compression curve is bi-linear, formed by a small compression (C_{ce1}) under low vertical stresses and a significant compression (C_{cp1}) under higher vertical stresses; (ii) when $\sigma_v > \sigma'_{v0}$ = 3.2 MPa, the compression curve progressively joins the virgin compression line defined by the common compression index C_c (see Figure 13).

For each unloading - reloading loop, two swelling stresses σ_s and four characteristic indices C_{se}, C_{sp}, C_{ce}, C_{cp} can be identified as illustrated in Figure 13. The yield stress σ'_y can be determined according to the French standard (AFNOR, 1997) as the stress value corresponding to the intersection between the virgin compression line and the line passing by point C (*in situ* state) with the slope C_{se1}.

Figure 14 shows that the swelling stress σ_s for each unloading/reloading path, in HPO and LPO tests, is well correlated with the corresponding initial void ratio e_i (the value before the unloading or reloading).

In addition, a series of swelling tests with "zero swell" method (Sridharan et al., 1986) was carried out by UCLouvain (1998) on Ypresian clays of several depths at the Doel site. Since the positions of Ypresian formation at Kallo (Cammaer et al., 2009) and Doel (Van Marcke & Laenen, 2005) are different, "equivalent depth" was used to compare data of the two sites. Given D_K a depth in Ypresian formation at Kallo, belonging to a member delimited by depth H_{1K} on the top and depth H_{2K} at the bottom, and the corresponding limit depths of this member at Doel are H_{1D} and H_{2D}, the "equivalent depth" of D_K at Doel (D_{KD}) can be determined as follows:

$$D_{KD} = \frac{D_K - H_{1K}}{H_{2K} - H_{1K}} \times \left(H_{2D} - H_{1D} \right) + H_{1D} \quad (1)$$

The swelling stress σ_s determined by "zero swell" method for the Ypresian clays at Doel at the equivalent depths, noted as YK43, 64, 73, 95-D, of the four studied cores are also presented in Figure 14 with the corresponding initial void ratio.

Linear relations between swelling stress σ_s and corresponding initial void ratio e_i are obtained in a semi-logarithmic plane for all the depths as observed by Cui et al. (2013). Moreover, good agreements between (i) Doel and Kallo sites (YK43 versus YK43-D and so on for YK64, 73 and 95), and (ii) common swelling tests and LPO and HPO compression tests are observed for each depth. For a given initial void ratio e_i, YK73 and YK95 (lower part of the Roubaix Member and upper part of the Orchies Member) show a significantly higher swelling stress σ_s as compared to YK43 and 64 (the upper part of the Roubaix Member).

The variations of C_{se} and C_{ce}, C_{sp} and C_{cp} with the preconsolidation stress σ'_p for each unloading/reloading path are presented in Figure 15a and b, respectively. For the first unloading and reloading loop, as the soil is only slightly over-consolidated (see paragraph below), σ'_p was

267 rounded to σ'_{v0} = 3.2 MPa for simplicity. For the second and third unloading-reloading loops,
268 based on the stress path in HPO tests, σ'_p was taken equal to 16 and 32 MPa, respectively. It
269 appears that C_{se} and C_{ce} are independent of the pre-consolidation stress σ'_p (Figure 15a) while
270 C_{sp} and C_{cp} increase with the increase of σ'_p. It is observed that these four indices are similar for
271 YK43 and YK64. It is also the case for those of YK73 and YK95. C_{se}, C_{sp} and C_{cp} of YK43 and
272 YK64 are much smaller than those of YK73 and YK95, C_{ce} being the same for the four samples.
273 Furthermore, for YK43 and YK64, the differences between C_{se} and C_{ce} and between C_{sp} and C_{cp}
274 are not obvious. On the contrary, for YK73 and YK95, for a given σ'_p, $C_{se} > C_{ce}$ and $C_{sp} < C_{cp}$.

275 The variation over depth of compression index C_c and yield stress σ'_y of Ypresian clays at Kallo,
276 determined according to Figure 13, are presented in Figure 16. The yield stress ratio *YSR* and the
277 over-consolidation ratio *OCR* are also reported in this figure. It is observed that the
278 compressibility of Ypresian clays increases with depth within the Roubaix Member (Figure 16a).
279 The yield stress σ'_y profile with indication of *YSR* and *OCR* (Figure 16b) shows a good
280 correspondence between the geological study undertaken by Van Marcke & Laenen (2005) and
281 this mechanical characterisation: the Ypresian clays are slightly over-consolidated and the *YSR*
282 for each depth is a little higher than the corresponding *OCR*. It also suggests that diagenesis as
283 well as other geological events after deposition are of minor importance for the Ypresian clays.

284 In addition, the long-term behaviour of the Ypresian clays was also investigated in this study
285 through the secondary compression/swelling coefficient $C_{\alpha e} = -\Delta e/\Delta \log t$. Considering the
286 important role of the swelling stresses σ_s on the compression curve e-logσ_v, a correlation
287 between $C_{\alpha e}$ with the ratio of vertical stress and swelling stress for the corresponding path σ_v/σ_s
288 (c.f. Figure 13) is analysed and presented in Figure 17 for both HPO and LPO tests. By

289 definition, $C_{\alpha e}$ is positive upon (re)loading and negative during unloading (see Deng et al.,
290 2012). It appears that for each depth a unique relationship ($C_{\alpha e}$, σ_v/σ_s) can be adopted for
291 different reloading (or unloading) paths of both HPO and LPO tests as sketch in the Figure 17.
292 Similarity in ($C_{\alpha e}$, σ_v/σ_s) between YK73 and 95 and between YK43 and 64 can be observed so as
293 only one trend line is adopted for the $C_{\alpha e}$ - σ_v/σ_s relation of each couple of cores in reloading (or
294 unloading). It is clearly observed that $C_{\alpha e}$ increases with the increase of σ_v/σ_s. Furthermore, for a
295 given σ_v/σ_s ratio, YK73 and YK95 show higher $C_{\alpha e}$, in absolute value, than YK43 and YK64.
296 Taking into account the large lifespan of a radioactive waste disposal as well as significant
297 delayed convergence monitored in URL galleries (Armand et al., 2013), these simple and
298 efficient correlations would be of considerable interest for further investigation and modelling of
299 the long-term behaviour of the geological barriers in the performance assessment framework.

300 *3.2. Permeability*

301 Based on the consolidation curves, the hydraulic conductivity k and permeability K were
302 determined based on the Casagrande's method:

303 $$k = \frac{C_v \rho_f g}{E_{oed}} \quad ; \quad K = \frac{k \mu_f}{\rho_f g} \tag{2}$$

304 where $C_v = 0.197H^2/t_{50}$ is the consolidation coefficient, H is the drainage length and t_{50} is the
305 time corresponding to 50% consolidation degree; ρ_f is the unit mass of fluid; g is the acceleration
306 due to gravity; $E_{\alpha d}$ is the œdometric modulus; and μ_f is the fluid dynamic viscosity.

307 The variations of hydraulic conductivity k and permeability K with void ratio are presented in
308 Figure 18. It appears that for a given void ratio, the soil permeability decreases with depth within

309 the range considered. In particular, the permeability of YK73 and 95 at their highest void ratio (e
310 $\approx$ 1) is still lower than that of YK43 at its lowest void ratio ($e \approx 0.5$).

311 A series of permeability tests under isochore condition on Ypresian clays at Doel was conducted
312 by Aertsens et al. (2005). The results are reported in Figure 19 for different depths. The values
313 obtained in this study for the Kallo site are also presented in Figure 19 using the "equivalent
314 depths" D_{KD} (see Eq. (1)). It can be observed that the results of the two studies are comparable
315 for the lower and the middle parts of the Roubaix Member. However, for YK43 the hydraulic
316 conductivity found in this study is significantly higher than that from Aertsens et al. (2005). This
317 shows some limitation of the comparison based on the notion of equivalent depth.

318 *3.3. Microstructure effect*

319 According to Mitchell & Soga (2005), the soil microstructure is defined by particle arrangement
320 and inter-particle bonding. Burland (1990) proposed a normalization method for the compression
321 curve e - $\log\sigma'_v$ which allows eliminating the effect of mineralogy and thus evidencing the effect
322 of microstructure. As reconstituted clays have similar microstructure (Burland, 1990; Leroueil et
323 al., 1985; Hong et al., 2010, 2012), their compression curves depend only on their mineralogy
324 characterised by their plasticity. These curves can be normalized using the void index I_v defined
325 by:

326 $$I_v = \frac{e - e^*_{100}}{e^*_{100} - e^*_{1000}} = \frac{e - e^*_{100}}{C^*_c} \quad (3)$$

327 where e^*_{100} and e^*_{1000} are the void ratios at σ_v' = 100 and 1000 kPa, respectively; $C^*_c = e^*_{100} - e^*_{1000}$ is
328 the compression index. These parameters can be empirically determined using the void ratio e_L at
329 liquid limit w_L (Burland, 1990; Chandler, 2000). The asterisk denotes properties of soils at

reconstituted state, considered as “intrinsic” and to be distinguished from the properties of soils at natural state that are affected not only by the mineralogy but also by microstructure.

By definition, all normalized compression curves I_v - $\log\sigma_v$ of reconstituted clays become a unique line passing by two points (0; 100 kPa) and (-1; 1000 kPa), namely intrinsic compression line - ICL (Figure 20). For natural clays, due to their microstructure developed along their geological history, their normalized compression curves lie on the right of ICL. Their positions depend on their sensitivity S_σ ranging generally from 1 for reconstituted soils to 10 (Cotecchia & Chandler, 2000). An average line at $S_\sigma = 5$ was defined as sedimentation compression line (SCL) by Burland (1990) and regarded as a typical relationship for marine sediments. Note that the sedimentation compression curve (SCC) of a natural soil, which can only be determined from the natural water content of undisturbed sample and thus cannot be reproduced in the laboratory, is not necessarily the SCL, neither the normalized compression curve determined by œdometer test.

The normalized compression curves of Ypresian clays are presented in Figure 20. The star symbols represent the *in situ* states. It appeared that differently from the *in situ* void ratio $e_{\sigma'v0}$, the *in situ* void index I_{v0} decreases with depth, and thus better represents the deposition process - the deeper the soil, the lower its *in situ* void index. Similar remark was made by Skempton (1970): the liquidity index $LI = (w - PL)/(LL - PL)$ is more representative of soil deposition process than water content w.

A significant difference between the *in situ* states of YK43 and the three lower depths (YK64, 73, 95) can be observed: while (I_{v0}, σ'_{v0}) for YK43 is situated between the SCL and ICL with an estimated SCC as indicated in Figure 20, the points (I_{v0}, σ'_{v0}) for (YK64, 73, 95) lie slightly below the ICL. Their SCCs must then coincide with the ICL because all the SCC of natural soils

must be on the right of the ICL or at least coincide with it. Due to these positions, the normalized compression curve of YK43 crosses its SCC before bending downward in parallel to the SCL and ICL, while the curves of (YK64, 73, 95) approach the ICL and then followed it. According to Baudet & Stallebrass (2004), the parallelism between the virgin compression curves and the SCL and ICL suggests that Ypresian clays have stable structure, as opposed to the soils of meta-stable structure which have virgin compression slopes steeper than those of SCL and ICL.

3.4. Microstructure after test

MIP test was conducted on the sample after test YK73O1, corresponding to the state at point H in Figure 11b. The pore size distribution (PSD) curve for this sample is presented in Figure 21. The PSD curve of intact YK73 sample is also reported in this figure for reference. It appears that after the HPO test, the nearly bi-modal PSD curve becomes almost a mono-modal one with a dominant pore diameter around D = 0.3 µm. It is observed that the infra-pores (Romero, 1999) with D < 0.02 µm were not affected by the test, while meso-pores (0.2 < D < 1 µm) increased in detriment of the micro-pores (0.02 < D < 0.2 µm) and the macro-pores (D > 1 µm). The pore-size family around D = 100 µm can also be explained by the technical perturbation during the preparation of samples as for the intact sample.

The SEM photos on the sample after test YK43O2, corresponding to the state at point F in Figure 9a, are presented in Figure 22, together with those on the intact sample YK43. On the whole, the bonded structure of the intact sample becomes less bounded after the mechanical loading in saturated condition with well distinguished silt grains.

4. Discussion

4.1. Physical and microstructural properties

The particle-size distribution (Figure 3) and mineralogical analyses (Table 1 and 2) by Vandenberghe (2011) showed that Ypresian clays are very fine-grained and highly plastic with significant amount of expansive minerals. These features are represented by their particularly high positions in the plasticity chart (Figure 4) and large values of initial void ratio e_0, specific surface S_s and *VBS* (Table 3) identified in this study and by Van Marcke & Laenen (2005). However there is a discrepancy between the results obtained by Vandenberghe (2011) and the results in the present study and Van Marcke & Laenen (2005) in terms of variability of these properties. Indeed, according to Vandenberghe (2011), the differences in particle-size distribution and especially in mineralogical composition for the Ypresian clays at Kallo are not significant between the four depths. On the contrary, clear distinctions in terms of physical and index properties between the two groups of depths – group 1: the middle of the Roubaix Member (YK43 and YK64) and group 2: the lower part of the Roubaix Member (YK73) and the upper part of the Orchies Member (YK95) (Figure 2) – were identified in the two latter studies: the upper group (group 1) shows higher density but lower grain density ρ_s, consistence indices *LL* and *PI*, specific surface S_s, blue methylene value *VBS* and water content w_0 than the lower group (group 2). Furthermore, these variations of ρ_s, *LL*, *PI*, *VBS*, S_s and w_0 are better in line with the geological history of Ypresian clays that is characterised by several transgressive - regressive cycles (see section 2.1). Further studies on the particle size distribution and mineralogy of Ypresian clays at Kallo are needed to clarify this point.

The SEM observations (Figure 5) also confirms the large difference between these two groups: the microstructure of the lower group is dominated by clay particles with matrix type, while that

of the upper group shows the dominance of silt grains with aggregate type. A progressive transition from the upper group to the lower one can be observed: the presence of clay fraction in YK64 is more obvious than in YK43 but still less than in YK73. Note that the carbonate content in YK43 (10 g/100g) is particularly higher than those in the three other depths. On the other hand, the PSDs of YK73 and probably YK95 (the lower group), show bi-modality with a dominant micro-pore family (D = 0.06 µm) at the intra-particle level and another dominant meso-pore family (D = 0.25 µm) at the inter-particle level; the PSD of YK43 is mono-modal with a sole dominant family of inter-particle pores having diameters as large as D = 0.8 µm. These microstructural differences are in good agreement with the macroscopic observations: the initial void ratio e_0 of the upper group are lower than those of the lower one that has higher plasticity.

4.2. Hydro-mechanical behaviour

The results of odometer tests of Ypresian clays with unloading - reloading cycles are characterised by clear hysteresis. According to Cui et al. (2013) and Nguyen (2013), these hysteretic loops can be explained by the competition between physico-chemical and mechanical effects that are separated by a threshold stress σ_s corresponding to the swelling stress. Note that the term “mechanical” refers to the particle interactions through their direct contact, while the term “physico-chemical” denotes the interactions between adsorbed water and clay particles. Upon unloading, when the applied external stress is higher than the swelling stress ($\sigma_v > \sigma_s$), or at the microscopic level the effect of the applied stress is stronger than that of the repulsive force between clay particles/sheets, the particles contact mode would be rather of face-to-face. As a result, the volumetric behaviour is rather controlled by the mechanical effect and small elastic rebound occurs. On the contrary, when $\sigma_v < \sigma_s$, the physico-chemical effect prevails as particles

contact turns progressively into face-to-edge mode, giving rise to soil swelling with significant volume change. Upon reloading, when the applied stress is lower than the swelling stress for this path $\sigma_v < \sigma_s$, the face-to-edge particles contact microstructure is more or less preserved due to the matrix suction caused by the physico-chemical effect, and small volume change occurs. By contrast, when $\sigma_v > \sigma_s$, the mechanical effect prevails and larger volume change occurs by collapse of large-pores, re-orienting particles contact to be more and more face-to-face mode. Beyond the preconsolidation stress $\sigma_v > \sigma'_p$, the plastic volume change makes the particle re-orientation more significant. Therefore, unloading from a higher preconsolidation stress σ'_p induces higher swelling slope C_{sp} (see Figure 15b).

4.2.1. Swelling capacity

The higher positions of the $\log\sigma_s$ - e_i curves of YK73 and YK95 with respect to those of YK43 and YK64 in Figure 14 clearly distinguish the two groups in terms of swelling stress σ_s. In addition, a unique correlation between e_i and σ_s may be expected with normalization by mineralogy, like the normalisation by dry density of bentonite in the case of bentonite mixtures (Agus, 2005; Dixon et al., 1996; Lee et al., 1999; Wang et al., 2012). Unfortunately, the discrepancy in mineralogical composition (Vandenberghe, 2011) and physical properties mentioned above does not allow this normalisation in the present study.

The increase of the swelling slope C_{sp} with the preconsolidation stress σ'_p (see Figure 15) confirms the enhanced physico-chemical effect by mechanical loading (Le et al., 2011): the larger the virgin compression, the more the orientation of clay particles (face-to-face particles contact mode) and thus the stronger the physico-chemical interaction between clay

439 particles and adsorbed water. The following equation can be proposed to describe the increase of
440 C_{sp} with σ'_p:

441
$$C_{sp(\sigma'_p)} = \frac{C_c}{1+\left(\frac{C_c}{C_{sp1}}-1\right)\times \exp^{-\beta \ln \frac{\sigma'_p}{\sigma'_{p1}}}} \quad (4)$$

442 where β is a parameter which controls the increase rate of C_{sp} with σ'_p. For YK43, 64, 73 and 95,
443 β = 0.22, 0.42, 0.35 and 0.35, respectively; σ_{p1} (= 3.25 MPa in this study) is a reference stress
444 corresponding to $C_{sp} = C_{sp1}$. The Eq. (4)-based correlations are shown by dotted lines in Figure
445 15b. It is observed that the values of C_{se} and C_{sp} as well as the slopes $\Delta C_{sp}/\Delta\sigma'_p$ of the two lower
446 depths (YK73 and 95) are larger than those of the two upper depths (YK43 and 64), despite the
447 lower densities of YK73 and 95. This again confirms the higher swelling capacity of YK73 and
448 95.

449 The independence of C_{se} with respect to σ'_p confirms that the soil behaviour during unloading
450 under $\sigma_v > \sigma_s$ is not significantly affected by the physico-chemical swelling, but characterised by
451 the mechanical rebounding. This justifies the yield stress σ'_y determination method adopted in
452 this study, avoiding inappropriate low values of σ'_y for deep sediments such as Boom Clay
453 (Baldi et al., 1991; Deng et al., 2011b; Sultan et al., 2010) and London clay (Gasparre, 2005).
454 Indeed, the values of σ'_y obtained in this study are in good agreement with the geological history
455 characterised by the values of *OCR*. The slightly higher values of *YSR* with respect to *OCR* can
456 reasonably be related to the creep effect developed during the geological history of several
457 millions of years. The larger difference between *YSR* and *OCR* for YK73 (1.6/1.1) and 95
458 (1.4/1.1) compared to those for YK43 (1.2/1.1) and 64 (1.5/1.2) (Figure 16b) indicates that creep

459 effect is more significant for the two lower cores than for the two upper ones. This is also
460 consistent with the higher swelling clay fraction of YK73 and YK95.

461 *4.2.2. Compressibility*

462 It is observed in Figure 15a that C_{ce} is independent of σ'_p and the mineralogy as the values are
463 quite similar for the four depths. This suggests that the microstructure characterised by the face-
464 to-edge particles contact mode that developed during the previous unloading was almost
465 preserved when $\sigma_v < \sigma_s$. This suggests also that the macroscopic volume change resulted mainly
466 from the compression of clay particles. Due to the competition between the increasing external
467 applied stress σ_v which tends to expel water from the clay particles and the physico-chemical
468 interaction between clay sheet and pore water which generates matrix suction retaining pore
469 water. The volume change in this stress range is thus negligible with $C_{ce} = 0.02$.

470 When the external applied stress is beyond the swelling stress $\sigma_v > \sigma_s$, the mechanical effect
471 prevails causing macro-pore collapse, giving rise to larger volume change with C_{cp}. Note that the
472 clay particle re-orientation in this stress range $\sigma_s < \sigma_v < \sigma'_p$ is less marked than in the virgin
473 compression domain where $\sigma_v > \sigma'_p$. Obviously, C_{cp} also increases with σ'_p and clay fraction as
474 observed in Figure 15. Moreover, the variation of C_{cp} must be limited by C_c on the upper side
475 and by C_{se} on the lower side because for a given σ'_p the higher the vertical stress σ_{vi} from which
476 the reloading is initiated, the lower the corresponding C_{cp}.

477 The increases of C_c (Figure 16a) and $C_{\alpha e}$ (Figure 17) with depth confirm the vertical variation of
478 the plasticity of Ypresian clays: the larger the consistence indices the larger the virgin and
479 secondary compression indices. This is in agreement with several correlations between
480 compression index and Atterberg limits in the literature for remoulded soils (Carrier, 1985;

Leroueil et al., 1984; Skempton, 1944; Terzaghi & Peck, 1967; Wroth & Wood, 1978) and also natural clayey soils (Johnson & Moston, 1970).

4.2.3. Permeability

The permeability evolution of Ypresian clays at the Kallo site with depth is also in agreement with the variations of soil mineralogy, grain-size distribution and microstructure: despite their higher void ratios, YK73 and 95 show significantly lower permeability than YK43 and 64. This can be explained by two reasons. From a microstructure point of view, the aggregate type fabric and the dominance of macro-pores in YK43 and 64 form larger flow channel than the matrix type fabric and the dominance of micro-pores in YK73 and 95 (Figure 6). From a mineralogical point of view, water molecules in clay particles are associated with the exchangeable cations adsorbed on the clay sheets forming the diffuse double layer. This affects the mobility of water molecules and thus the permeability. Indeed, YK43 and 64 have similar void ratio (Table 4) and microstructure type (Figure 5), but YK64 clearly shows lower permeability (Figure 18) because of its higher plasticity index (Figure 4).

4.3. Microstructure effect on volumetric behaviour

The significantly higher positions of the *in situ* state (I_{v0}, σ'_{v0}) and the normalized compression curve of YK43 with respect to those of YK64, 73 and 95 in the I_v - $\log\sigma_v$ plane can be related to its lower clay fraction as observed on the SEM photos (Figure 5) and in the plasticity chart (Figure 4), and its higher carbonate content (Table 3) which plays a decisive role in inter-particle bonding. With the highest plasticity index and the lowest carbonate content, the normalized compression curve of YK73 is logically the lowest one. The curve of YK95 is close to that of

YK73 albeit its higher carbonate content (3.8 against 0.9 g/100 g). This suggests that the effect of carbonates in the microstructure can be compensated by that of expansive clay minerals.

According to Burland (1990), the stable microstructure of Ypresian clays (virgin compression curves have the same slope as the SCL and ICL) indicates a quick deposition from a dense suspension and/or under strong current. These depositional conditions would give rise to a more oriented fabric thus more compact with a low void index I_v (not necessarily low void ratio e).

Particularly high expansive mineral content could also be the reason for the evolution of the PSD curve, from nearly bi-modal for intact YK73 sample to nearly mono-modal for the sample after the HPO test (Figure 21). Indeed, under compression at high pressures, clay particles were re-oriented and fill the meso- and macro-pores. The porosity under high pressures became more and more homogeneous with a sole dominant micro-pores. Upon unloading, due to the effect of expansive minerals, the uniformity of the porosity was preserved as the dominant micro-pore family swelled homogeneously to reach the size of meso-pores. On the contrary, due to the limited amount of clay minerals, after the LPO test, the aggregate type microstructure of YK43 became even clearer as clay particles were only able to coat the silt grains, but not enough to form a matrix. Therefore, the swelling upon unloading from $\sigma_v = \sigma'_{v0}$ consisted mainly in the rebounding of the "frame structure" built by clay-coated silt grains, which is different from the volume change mode of YK73. Thus, the void ratios at the end of the first unloading (point D) in both LPO and HPO tests are much lower than the initial value $e_D < e_0$ for YK43 (Figure 9), but higher than the initial value $e_D > e_0$ for YK73 (Figure 11).

5. Conclusion

The physical and geotechnical identifications, microstructure analysis and œdometer tests with unloading-reloading loops have been performed on the samples of Ypresian clays cored at Kallo

525 (N-Belgium) in order to assess the Ypresian clays as a potential host formation for geological
526 disposal of radioactive wastes. Ypresian clays have been identified as fine-grained soil, highly
527 plastic, particularly porous with respect to their depths, and slightly carbonated except core
528 YK43.

529 Significant variability in terms of physical and geotechnical properties and microstructure have
530 been identified: i) the middle of the Roubaix Member (cores YK43 and YK64) presents lower
531 plasticity indices, void ratio e_0, water content w_0 and higher density ρ_0 than the lower part of the
532 Roubaix Member (core YK73) and the upper part of the Orchies Member (core YK95); ii) the
533 microstructure of core YK43 (middle of the Roubaix Member) is characterized by the aggregate
534 type with dominance of the silty grains and a sole dominant meso-pore family at D = 0.8 µm.
535 The microstructure of core YK73 (lower part of the Roubaix Member) shows presence of a clay
536 matrix in which are dispersed silty grains, forming a bi-modal porosity with dominant micro-
537 pore (D = 0.06 µm) and meso-pore (D = 0.25 µm) families.

538 The œdometer compression curves of Ypresian clays are characterised by typical unloading -
539 reloading hysteretic loops, commonly observed for fine-grained soils in the literature. This
540 feature have been interpreted, according to Cui et al. (2013), by the competition between the
541 mechanical and physico-chemical effects which are separated by a swelling stress. This approach
542 allowed (i) properly determining the yield stress σ'_y of Ypresian clays at Kallo, which are in
543 good agreement with their geological history; (ii) better identifying the swelling capacity as well
544 as its dependence on their loading history. A semi-logarithmic linear relationship between the
545 swelling stress and initial void ratio, determined by common swelling tests and œdometer
546 compression tests were obtained. This confirmed the swelling stress concept proposed by Cui et

al. (2013) and showed the consistency between the different tests performed in this study as well as the tests reported by Van Marcke & Laenen (2005).

The mechanical and hydraulic parameters deduced from œdometer tests showed significant variation over depth: the compressibility and swelling capacity increases while the hydraulic conductivity decreases over depth despite the increasing porosity. The normalised compression curves in the I_v - $\log\sigma_v$ plane properly described the deposition process: the deeper the soil, the lower its *in situ* void index I_{v0}. In addition, the Ypresian clays are characterised by stable microstructure. The high carbonate content and aggregate type microstructure of YK43 were also well identified by the distinct position of its I_v - $\log\sigma_v$ curve from those of the three other samples in the ICL-SCL framework.

6. References

Aertsens, M., Dierckx, A., Put, M., Moors, H., Janssen, K., Van Ravestyn, L., De Cannière, P., 2005. Determination of the hydraulic conductivity, ηR and the apparent diffusion coefficient on Ieper Clay and Boom Clay cores from the Doel-l and Doel-2b drillings. Report No. SCK-CEN-R-3589 02/MAe/P-9, SCK-CEN.

AFNOR., 1997. Essai de compressibilité sur matériaux fins quasi saturés avec chargement par paliers. XP P 94-090-1 (Vol. 1).

AFNOR., 1998. Mesure de la capacité d'adsorption de bleu de méthylène d'un sol ou d'un matériau rocheux. Détermination de la valeur de bleu de méthylène d'un sol ou d'un matériau rocheux par l'essai à la tache. NF P 94-068.

Agus, S., 2005. An experimental study on hydro-mechanical characteristics of compacted

bentonite-sand mixtures. Bauhaus-University Weimar.

Armand, G., Noiret, A., Zghondi, J., Seyedi, D.M., 2013. Short- and long-term behaviors of drifts in the Callovo-Oxfordian claystone at the Meuse/Haute-Marne Underground Research Laboratory. *Journal of Rock Mechanics and Geotechnical Engineering, 5*, 221-230.

ASTM., 2006. Standard Practice for Classification of Soils for Engineering Purposes (Unified Soil Classification System). ASTM D 2487 - 06.

Baldi, G., Hueckel, A., Peano, A., Pellegrini, R., 1991. *Developments in modelling of thermo-hydro-geomechanical behaviour of Boom clay and clay-based buffer materials* (No. EUR 13964 EN). Commission of the European Communities.

Baudet, B., Stallebrass, S., 2004. A constitutive model for structured clays. *Géotechnique, 54*(4), 269-278.

Burland, J.B., 1990. On the compressibiity and shear strength of natural clays. *Géotechnique, 40*(3), 329–378.

Cammaer, C., Cockaerts, G., Schiltz, M., 2009. *Drilling and géological report ON-KALLO-1, ON-KALLO-2, ON-KALLO-3* (No. Samsuffit R2009-01). ONDRAF/NIRAS.

Carrier, W. D. (1985). Consolidation Parameters Derived From Index Tests. *Geotechnique, 35*(2), 211-213.

Chandler, R.J., 2000. Clay sediments in depositional basins: the geotechnical cycle (The 3rd Glossop Lecture). *Quarterly Journal of Engineering Geology and Hydrogeology, 33*(1), 5-39.

590 Coll, C., 2005. Endommagement des roches argileuses et perméabilité induite au voisinage
591 d'ouvrage souterrains. Université Joseph Fourier-Grenoble 1, Grenoble.

592 Cotecchia, F., Chandler, R.J., 2000. A general framework for the mechanical behaviour of clays.
593 *Géotechnique, 50*(4), 431-447.

594 Cui, Y.J., Nguyen, X.P., Tang, A.M., Li, X.L., 2013. An insight into the unloading/reloading
595 loops on the compression curve of saturated clays. *Applied Clay Science, 83-84*, 343-348.

596 Dehandschutter, B., Vandycke, S., Sintubin, M., Vandenberghe, N., Gaviglio, P., Sizun, J.P.,
597 Wouters, L., 2004. Microfabric of fractured Boom Clay at depth: a case study of brittle–
598 ductile transitional clay behaviour. *Applied Clay Science, 26*, 389-401.

599 Delage, P., Le, T.T., Tang, A.M., Cui, Y.J., Li, X.L., 2007. Suction effects in deep Boom Clay
600 block samples. *Géotechnique, 57*, 239-244.

601 Deng, Y.F., Cui, Y.J., Tang, A.M., Nguyen, X.P., Li, X.L., Van Geet, M., 2011a. Investigating
602 the pore-water chemistry effects on the volume change behaviour of Boom clay. *Physics*
603 *and Chemistry of the Earth, 36*, 1905- 1912.

604 Deng, Y.F., Tang, A.M., Cui, Y.J., Nguyen, X.P., Li, X.L., Wouters, L., 2011b. Laboratory
605 hydro-mechanical characterisation of Boom Clay at Essen and Mol. *Physics and*
606 *Chemistry of the Earth, 36*, 1878- 1890.

607 Deng, Y.F., Tang, A.M., Cui, Y.J., Li, X.L., 2011c. Study on the hydraulic conductivity of Boom
608 clay. *Canadian Geotechnical Journal, 48*, 1491-1470.

609 Deng, Y.F., Cui, Y.J., Tang, A.M., Li, X.L., Sillen, X., 2012. An experimental study on the
610 secondary deformation of Boom Clay. *Applied Clay Science, 59-60*, 19-25.

611 Dixon, D.A., Gray, M.N., Graham, J., 1996. Swelling and hydraulic properties of bentonites
612 from Japan, Canada and USA (pp. 5-8). Presented at the second International Congress
613 on Environmental Geotechnics, Osaka, Japan.

614 Gasparre, A., 2005. Advanced laboratory characterisation of London clay. Imperial College
615 London.

616 Hong Z.S., Yin J., Cui Y.J., 2010. Compression Behaviour of Reconstituted Soils at High Initial
617 Water Contents. *Géotechnique, 60(9),* 691-700.

618 Hong Z.S., Zeng L.L., Cui Y.J., Cai Y.Q., Cheng L., 2012. Compression Behaviour of Natural
619 and Reconstituted Clays. *Géotechnique, 62*(4), 291-301.

620 Johnson, A.I., Moston, R.P., 1970. Relationship of consolidation characteristics and Atterberg
621 limits for subsiding sediments in central California, USA. Presented at the International
622 Symposium on Land Subsidence.

623 Le, T.T., Cui, Y.J., Munoz, J.J., Delage, P., Tang, A.M., Li, X.L., 2011. Studying the stress-
624 suction coupling in soils using an oedometer equipped with a high capacity tensiometer.
625 *Front. Archit. Civ. Eng. China*, *5*(2), 160-170.

626 Lee, J.O., Cho, W.J., Chun, K.S., 1999. Swelling Pressures of a Potential Buffer Material for
627 High-Level Waste Repository. *Journal of the Korean Nuclear Society, 31,* 139- 150.

628 Leroueil, S., Tavenas, F., Locat, J., 1984. Correlations between index tests and the properties of
629 remoulded clays. *Géotechnique, 35*(2), 223-229.

630 Leroueil, S., Tavenas, F., Locat, J., 1985. Discussion: Correlations between index tests and the
631 properties of remoulded clays. W. D. Carrier and J. F. Beckman. *Géotechnique, 35*(2),
632 223-226.

633 Lima, A., 2011. Themo-Hydro-Mechanical behaviour of two deep Belgian clay formations:
634 Boom and Ypresian clays. Universitat Politècnica de Catalunya, Spain.

635 Mitchell, J. K., Soga, K., 2005. *Fundamentals of soil behavior*. John Wiley & Sons, Inc.

636 Nguyen, X.P., 2013. Étude du comportement chimico-hydro-mécanique des argiles raides dans
637 le contexte du stockage géologique de déchets radioactifs. Ecole des Ponts ParisTech.

638 ONDRAF, 2001. Safety Assessment and Feasibility Interim Report 2 (No. SAFIR2).NIROND
639 2001-06.

640 Romero, M.E., 1999. Characterisation and thermo-hydro-mechanical behaviour of unsaturated
641 Boom clay: an experimental study. Universitat Politècnica de Catalunya.

642 Skempton, A.W., 1944. Notes on the Compressibility of Clays.". *Q. J. Geol. Soc. London*, *100*(1-
643 4), 119-135.

644 Skempton, A.W., 1970. The consolidation of clays by gravitational compaction. *Q. J. Geol. Sot.*,
645 *125*, 373-411.

646 Sridharan, A., Rao, A.S., Sivapullaiah, P.V., 1986. Swelling pressure of clay. *Geotechnical*
647 *Testing Journal*, *9*(1), 24-31.

648 Sultan, N., Cui, Y.J., Delage, P., 2010. Yielding and plastic behaviour of Boom Clay.
649 *Géotechnique, 60*(9), 657-666.

650 Terzaghi, K., Peck, R.B., 1967. *Soil Mechanics in Engineering Practice*. John Wiley London.

651 Tran, N.L., 1980. L'essai au bleu de méthylène Un progrès dans la mesure et le contrôle de la
652 propreté des granulats. *Bulletin de liaison des laboratoires des ponts et chaussées*, *107*,
653 130-135.

UCLouvain, 1998. *Rapport d'essai forage Doel-1A*. Laboratoire du Génie Civil, Université Catholique de Louvain.

Van Marcke, P., 2009. Existing information on the Ypresian clays. In *Meeting on the THMC characterisation of Ypresian clays*.

Van Marcke, P., Laenen, B., 2005. The Ypresian clay as possible host rock for radioactive waste disposal: An evaluation. ONDRAF.

Vandenberghe, N., 2011. Qualitative & quantitative mineralogical analyses of Ypresian clay. KULeuven.

Wang, Q., Tang, A.M., Cui, Y.J., Delage, P., Gatmiri, B., 2012. Experimental study on the swelling behaviour of bentonite/claystone mixture. *Engineering Geology*, *124*(1), 59-66.

Wroth, C.P., Wood, D.M., 1978. The correlation of Index Properties with Some Basic Engineering Properties of Soils. *Canadian Geotechnical Jounal*, *15*, 137-145.

668 **7. List of tables**

669 Table 1: Mineralogical composition of Ypresian clays in bulk mass (after Vandenberghe, 2011)

670 Table 2: Mineralogical composition of Ypresian clays in clay-size fraction (after Vandenberghe,
671 2011)

672 Table 3: Physical properties of Ypresian clays

673 Table 4: Test program

674 **8. List of figures**

675 Figure 1: Thickness and depth of the top of Kortrijk formation (After ONDRAF, 2001)

676 Figure 2: Stratigraphical profile and system track of Ypresian clays at Kallo and soil core
677 positions, modified from Cammaer et al. (2009) and Van Marcke & Laenen (2005)

678 Figure 3: Particle-size distribution curves (after Vandenberghe, 2011)

679 Figure 4: Classification of Ypresian clays at Doel and Kallo

680 Figure 5: SEM photos of Ypresian clays at Kallo

681 Figure 6: Pore-size distribution curves of Ypresian clays

682 Figure 7: Vertical stress and displacement variations in high-pressure œdometer test

683 Figure 8: Vertical stress and displacement variations in low-pressure œdometer test

684 Figure 9: Low- (a) and high- (b) pressure œdometer compression curves on YK43

685 Figure 10: Low- (a) and high- (b) pressure œdometer compression curves on YK64

686 Figure 11: Low- (a) and high- (b) pressure œdometer compression curves on YK73

687 Figure 12: Low- (a) and high- (b) pressure œdometer compression curves on YK95

688 Figure 13: Parameter definitions

689 Figure 14: Swelling stress σ_s versus (initial) void ratio (*ei*) *e* for Ypresian clay

690 Figure 15: Variations of C_{se}, C_{ce} (a), C_{sp} and C_{cp} (b) versus preconsolidation stress σ'_p

691 Figure 16: Compression index C_c (a) and yield stress σ'_y (b) profiles

692 Figure 17: Secondary compression/swelling coefficient

693 Figure 18: Permeability of Ypresian clays

694 Figure 19: Hydraulic conductivity profile for Ypresian clays at Doel (after Aertsons et al., 2005)

695 Figure 20: Normalized compression curves

696 Figure 21: Pore-size distribution curves of intact and after HPO test YK73

697 Figure 22: SEM on intact (left) and after LPO test (right) YK43

698

699

700 **Table 1: Mineralogical composition of Ypresian clays in bulk mass (after Vandenberghe, 2011)**

Core	Depth (m)	Non-clay minerals (wt %)					Clay minerals (wt %)				
		Qtz	Feld.	Car.	Others	Σ_{NC}	Kaol.	Chl.	Sm. Eq.	Ill. Eq.	Σ_C
YK44	331.48	32	12	2	0.4	46	2	3	33.7	15.3	54
YK63	350.41	36	13	1.7	1.7	52	5	3	30.8	9.2	48
YK74	361.29	31	11	0.8	0.4	43	3	4	28.8	21.2	57
YK96	383.01	27	10	4	0.8	42	3	3	30.4	22.6	59

701

702 **Table 2: Mineralogical composition of Ypresian clays in clay-size fraction (after Vandenberghe, 2011)**

Core	Relative to clay-size fraction (wt %)								Relative to total mass (wt %)				
	Ill.-Sm. (wt %)	(%Sm.)	Ill.	Sm.	Kaol.	Chl.	ΣSm.	Σ2:1	Σ2:1	Ill.-Sm.	Ill.	Sm.	ΣSm.
YK44	24	38	9	63	2	2	72	96	49	12	5	32	37
YK63	24	33	9	62	1	4	70	95	40	10	4	26	29
YK74	22	38	10	63	2	3	71	95	50	12	5	33	38
YK96	23	37	10	59	3	5	68	92	53	13	6	34	39

703 *Qtz: Quartz; Feld.: Feldspar; Car.: Carbonates; Others: Plagioclase, dolomite, Pyrite, Anatase, Opal CT and*
704 *Zeolite; Σ_{NC}: Total non-clay minerals; Kaol.: Kaolinite; Chl.: Chlorite; Sm. Eq. = equivalent of smectite in the bulk*
705 *rock based on the CEC results assuming an average smectite with a charge of 100meq/100g; Ill. Eq. = equivalent of*
706 *illite(/muscovite) in the bulk rock calculated as Σ2:1 - sm. Eq; Σ2:1: di-octahedral clays (illite, smectite, illite-*
707 *smectite, glauconite) and micas; ΣC: Total clay minerals; ΣSm. = Sm. + Ill.-Sm.×%Sm., is the total smectite content*

708

709

710

711

712

713

714

715

716 **Table 3: Physical properties of Ypresian clays**

Core	YK43	YK64	YK73	YK95
G_s (-)	2.776	2.785	2.802	2.802
ρ_0 (Mg/m^3)	1.97 ± 0.03	1.97 ± 0.01	1.9 ± 0.01	1.91 ± 0.05
ρ_{d0} (Mg/m^3)	1.57	1.55	1.43	1.47
e_0 (-)	0.77 ± 0.03	0.79 ± 0.03	0.95 ± 0.06	0.90 ± 0.06
n_0 (%)	44 ± 1.1	44 ± 1.1	49 ± 1.6	47 ± 1.5
LL (-)	75.07	113.84	136.61	132.22
PL (-)	33.50	33.75	36.08	43.75
PI (-)	41.57	80.09	100.53	88.47
w_0 (%)	25.78 ± 0.73	26.74 ± 1.86	32.01 ± 1.56	29.78 ± 1.94
S_{r0} (%)	93 ± 3	95 ± 4	96 ± 4	93 ± 5
S_s (m^2/g)	83	149	275	267
VBS (g/100 g)	3.95	7.09	13.12	12.72
% $CaCO_3$ (g/100 g)	10.2	1.4	0.9	3.8

717
718
719 **Table 4: Test program**

Core	Test	w_0 (%)	e_0 (-)	n_0 (%)	S_{r0} (%)	ρ_0 (Mg/m^3)	$e_{\sigma'v0}$ (-)
43	YK43O1	26.04	0.81	45	89	1.94	0.70
	YK43O2	25.05	0.78	44	89	1.95	0.64
64	YK64O1	26.22	0.79	44	92	1.96	0.74
	YK64O2	27.65	0.80	44	97	1.98	0.73
73	YK73O1	31.09	0.94	48	93	1.89	0.82
	YK73O2	31.36	0.93	48	95	1.91	0.80
95	YK95O1	29.72	0.95	49	87	1.86	0.80
	YK95O2	31.73	0.94	49	94	1.90	0.80

720

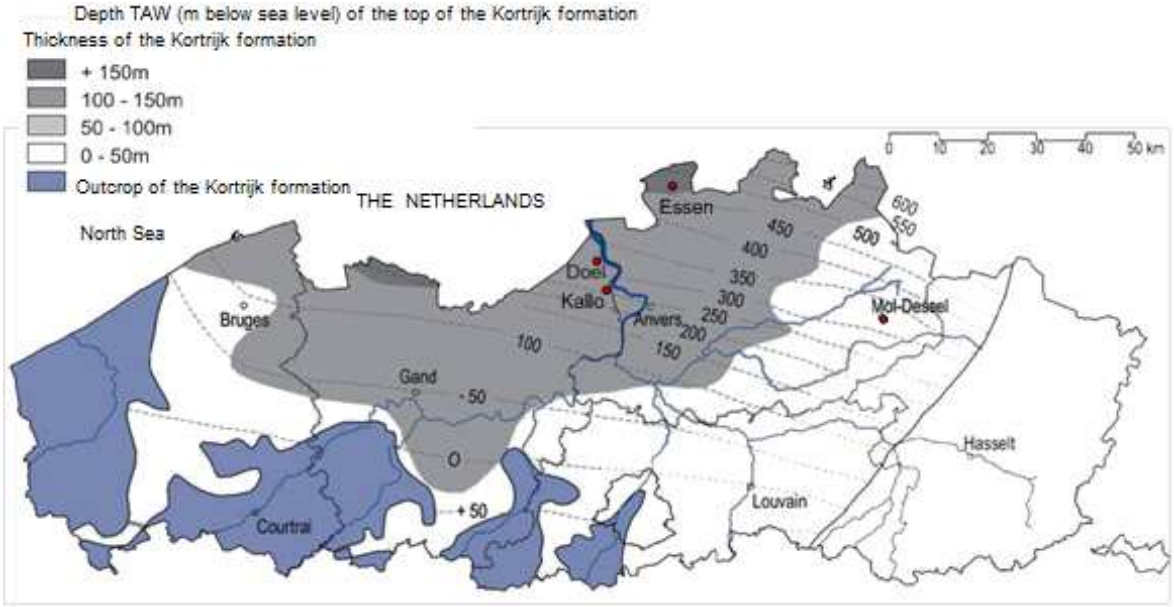


Figure 1: Thickness and depth of the top of Kortrijk formation (After ONDRAF, 2001)

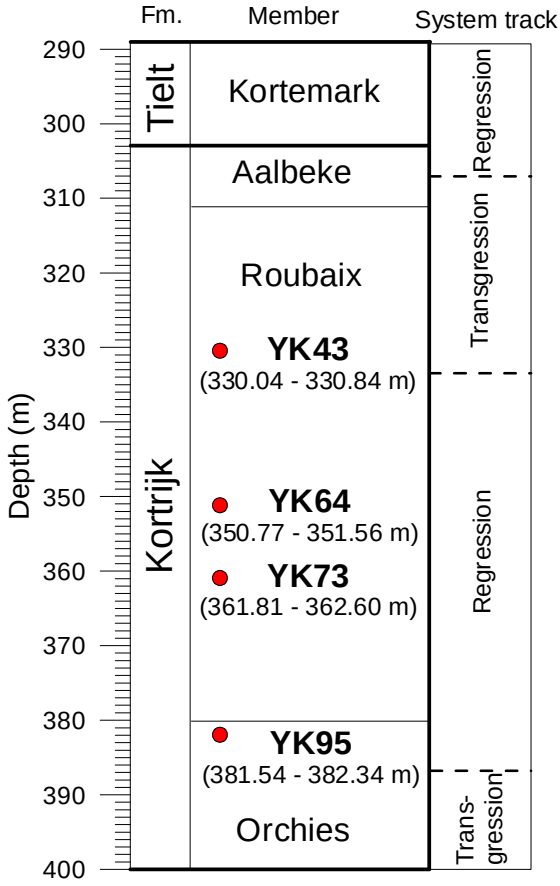
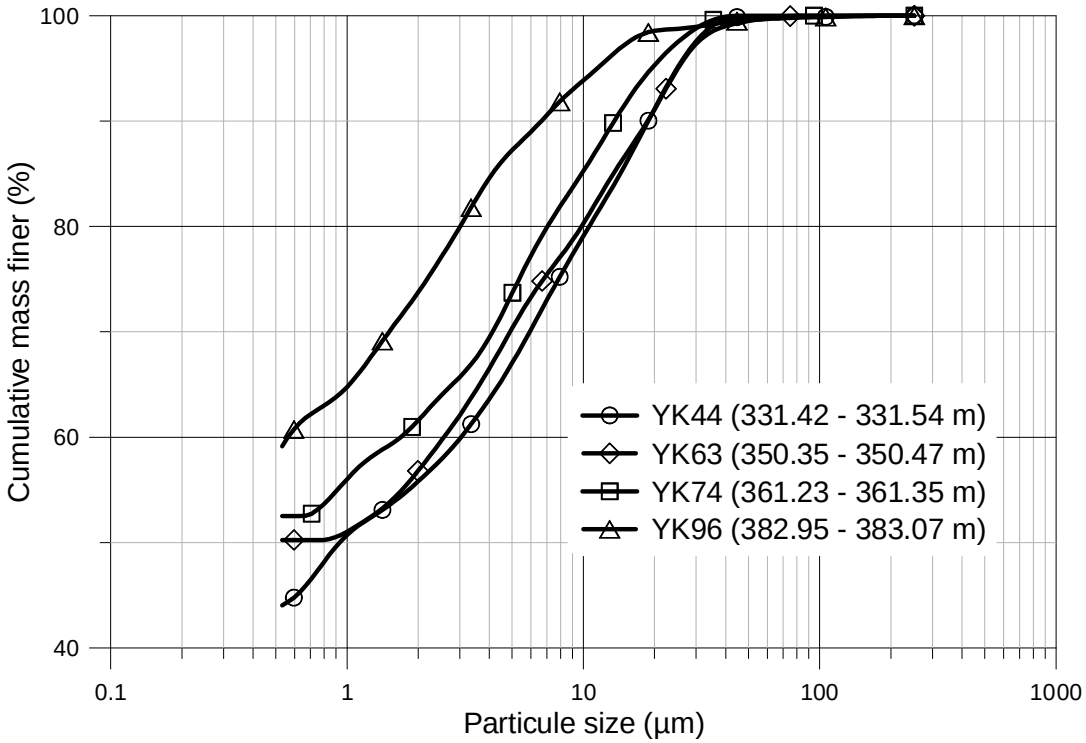
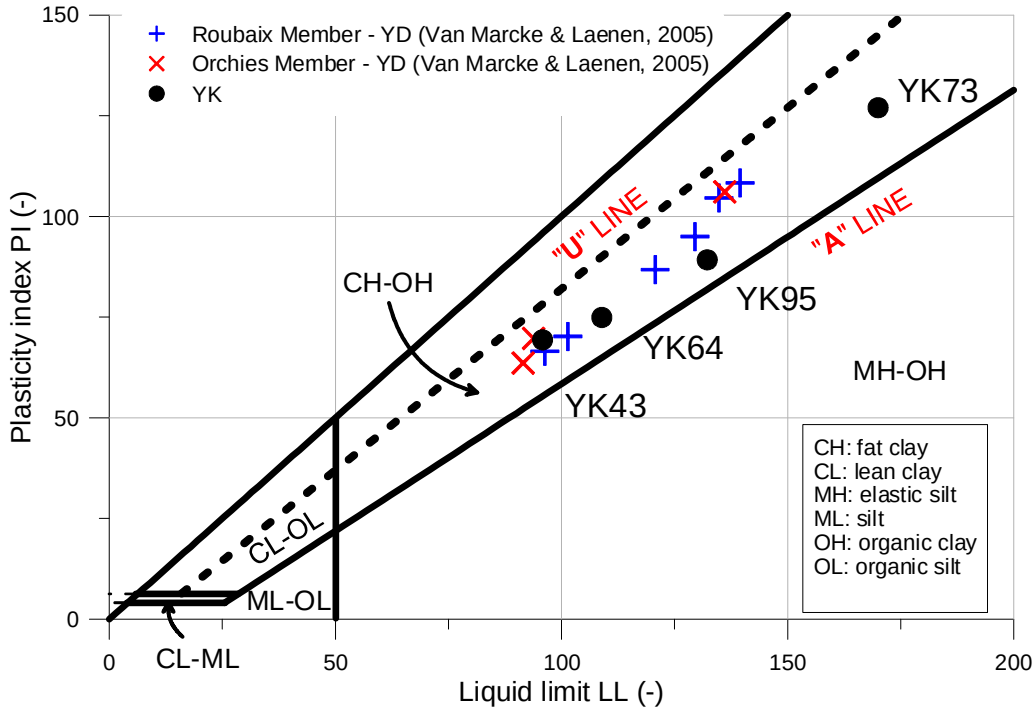


Figure 2: Stratigraphical profile and system track of Ypresian clays at Kallo and soil core positions, modified from Cammaer et al. (2009) and Van Marcke & Laenen (2005)



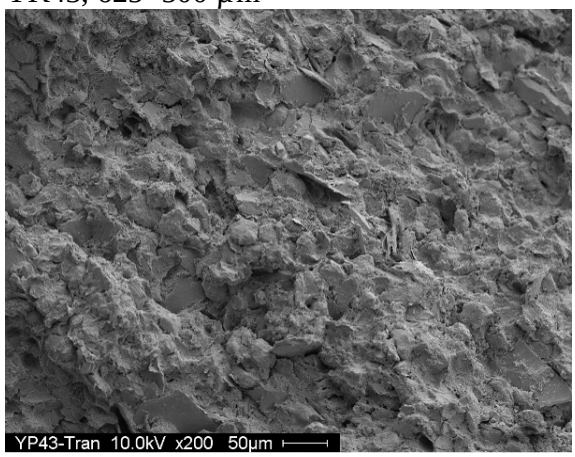
729
730 **Figure 3: Particle-size distribution curves (after Vandenberghe, 2011)**

731

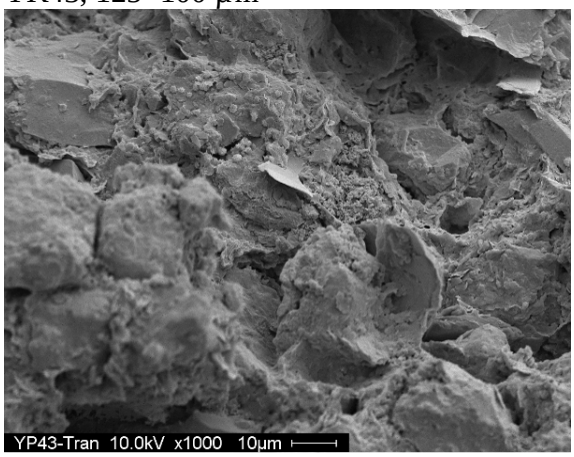


732
733 **Figure 4: Classification of Ypresian clays at Doel and Kallo**

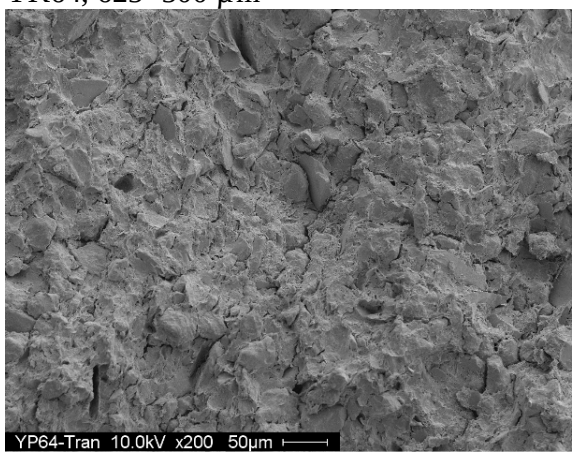
YK43, 625×500 µm



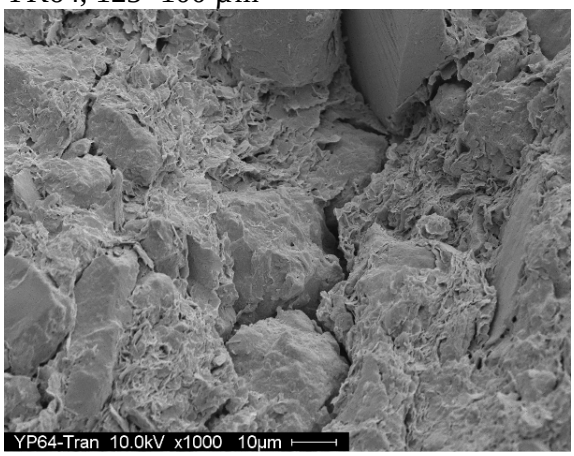
YK43, 125×100 µm



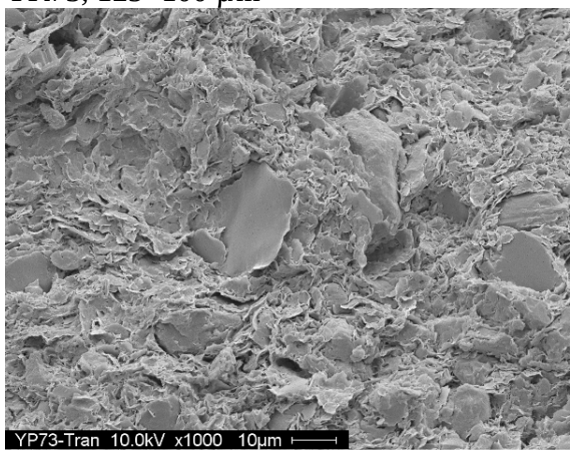
YK64, 625×500 µm



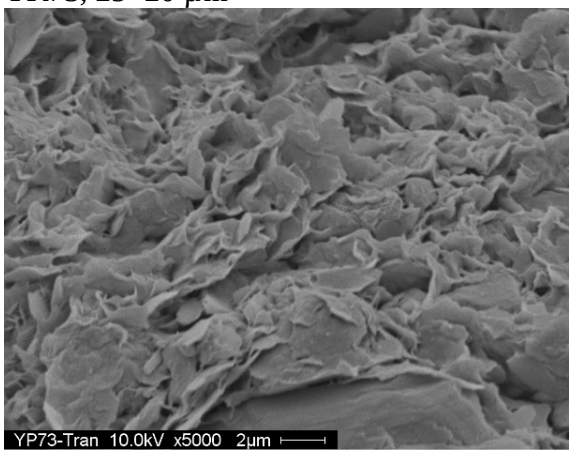
YK64, 125×100 µm



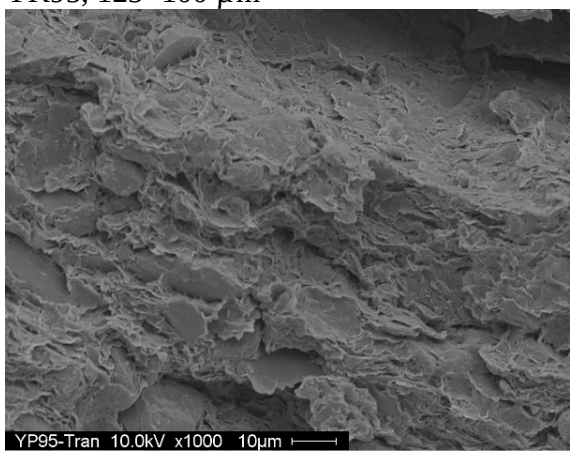
YK73, 125×100 µm



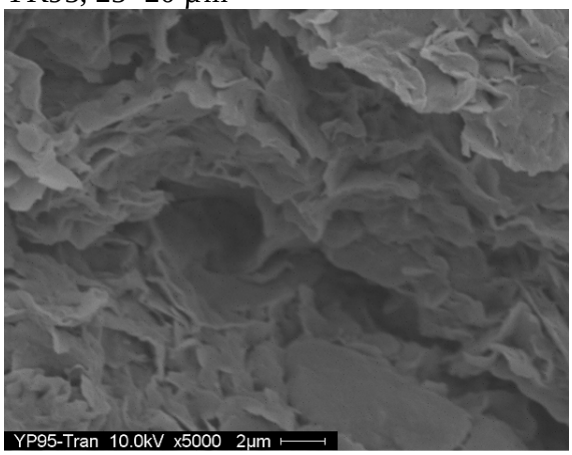
YK73, 25×20 µm



YK95, 125×100 µm

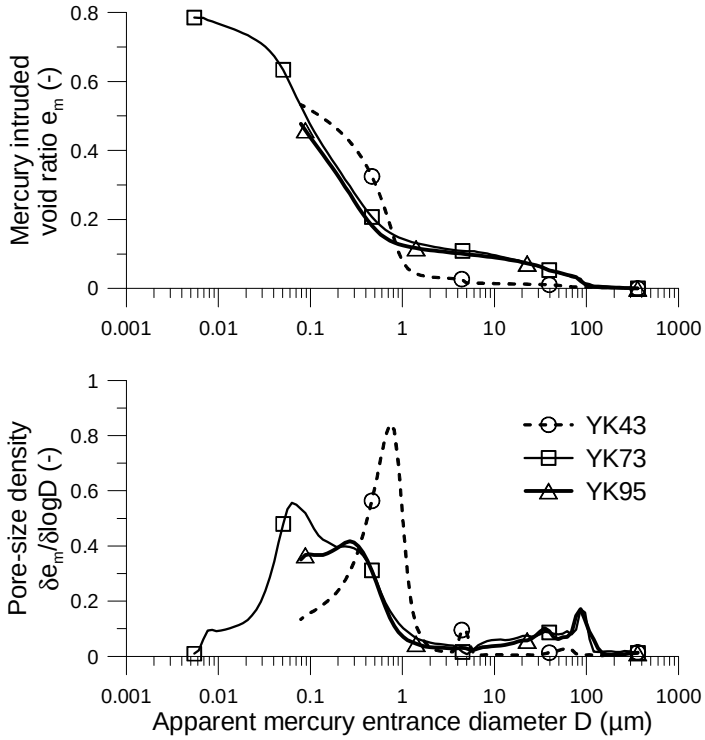


YK95, 25×20 µm



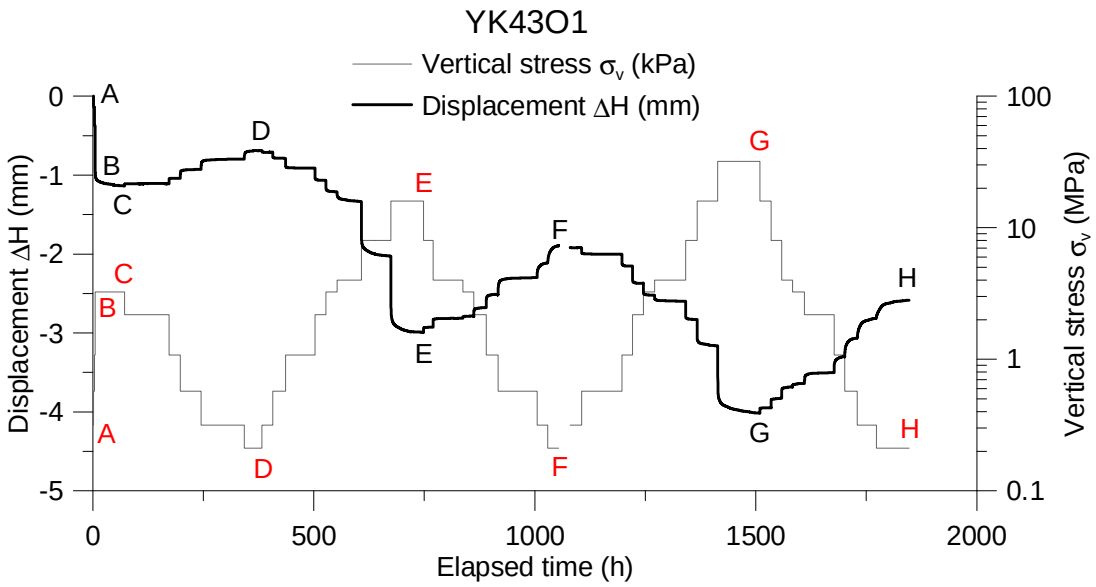
734 **Figure 5: SEM photos of Ypresian clays at Kallo**

735



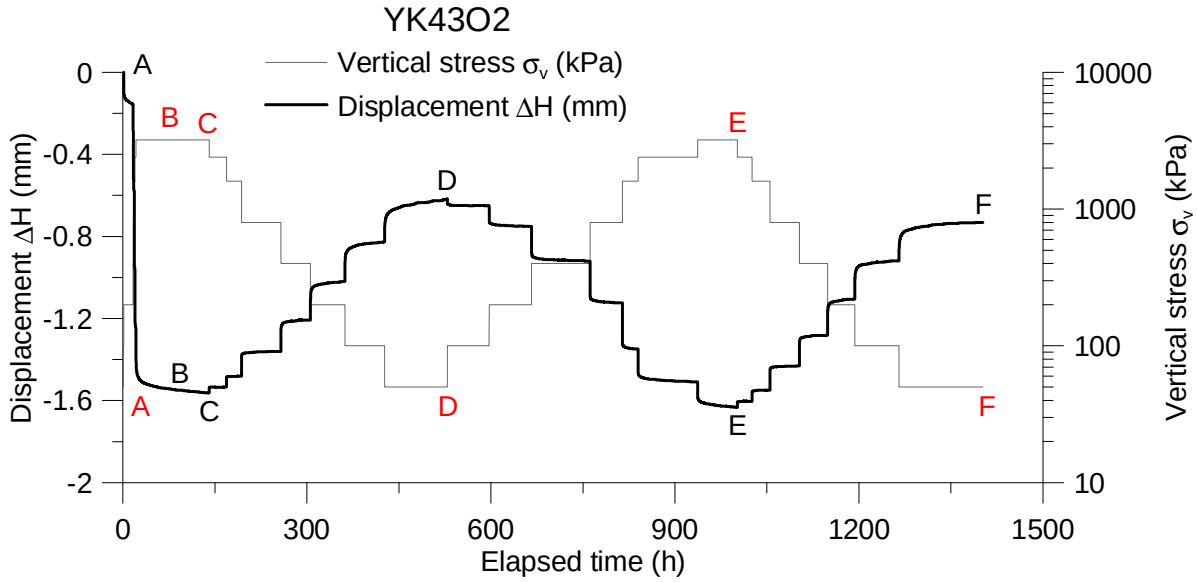
736
737 **Figure 6: Pore-size distribution curves of Ypresian clays**

738



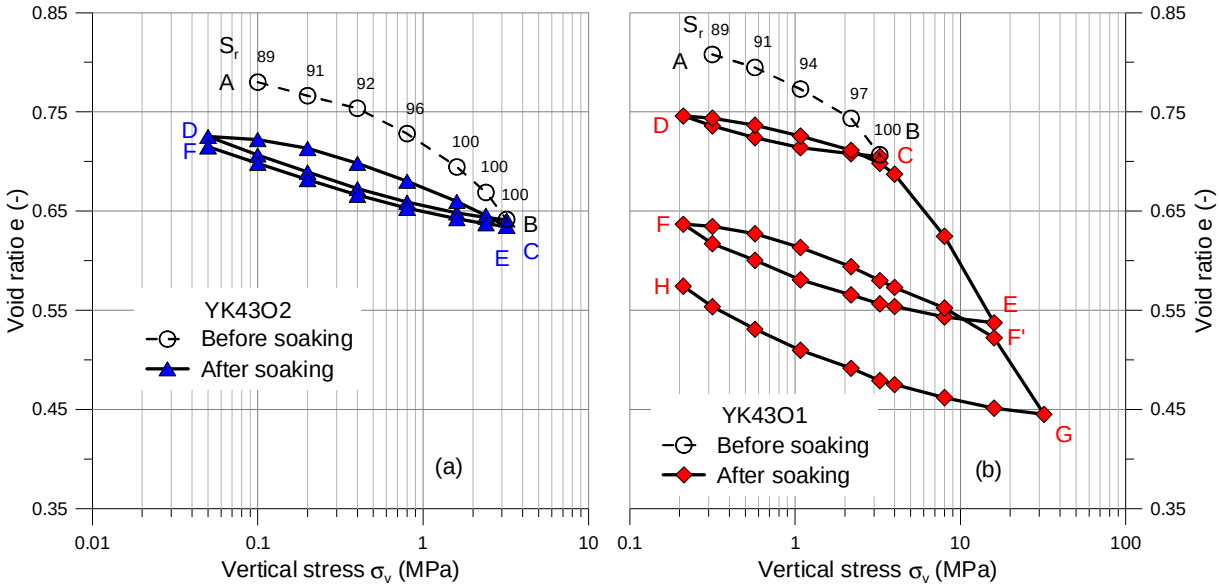
739
740 **Figure 7: Vertical stress and displacement variations in high-pressure œdometer test**

741



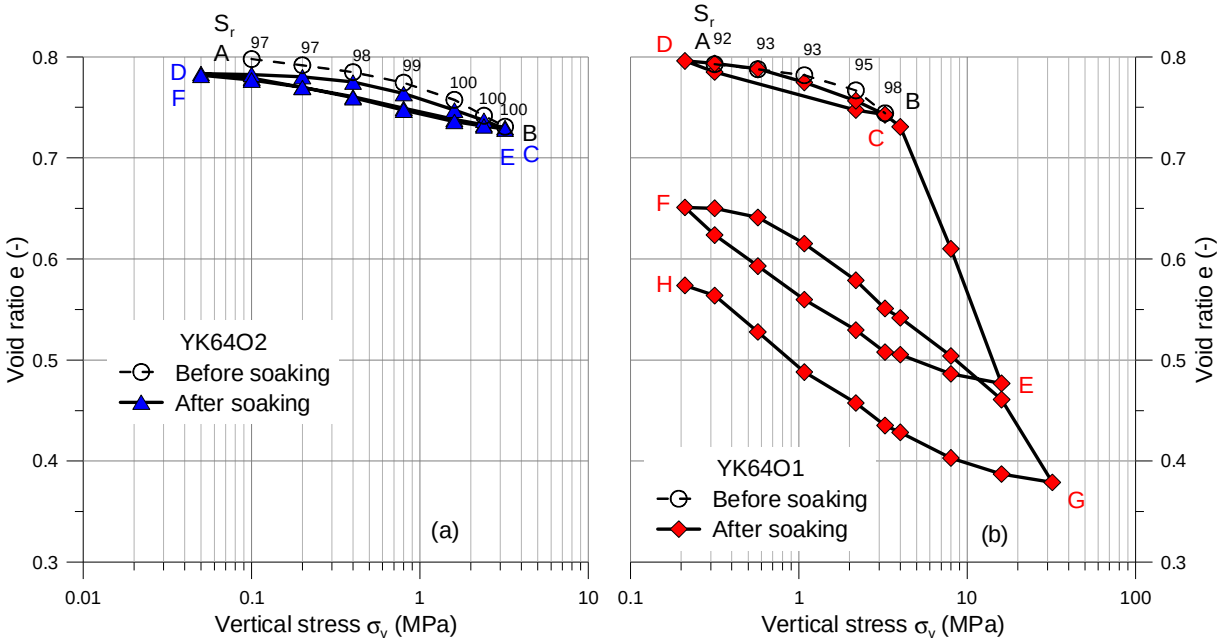
742
743 **Figure 8: Vertical stress and displacement variations in low-pressure œdometer test**

744



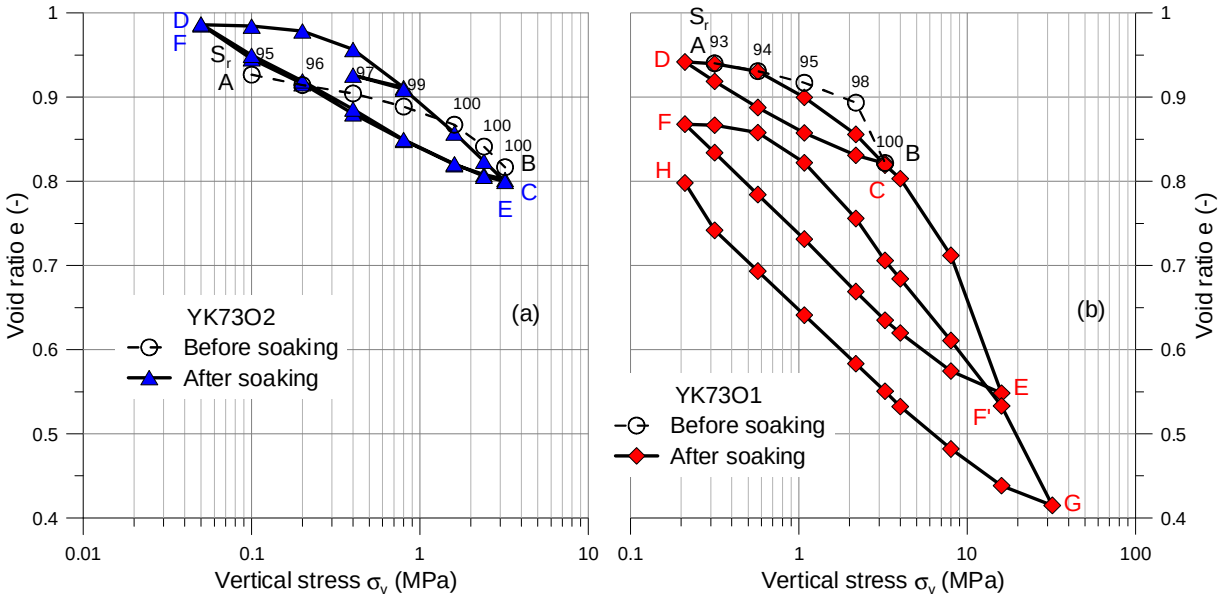
745
746 **Figure 9: Low- (a) and high- (b) pressure œdometer compression curves on YK43**

747



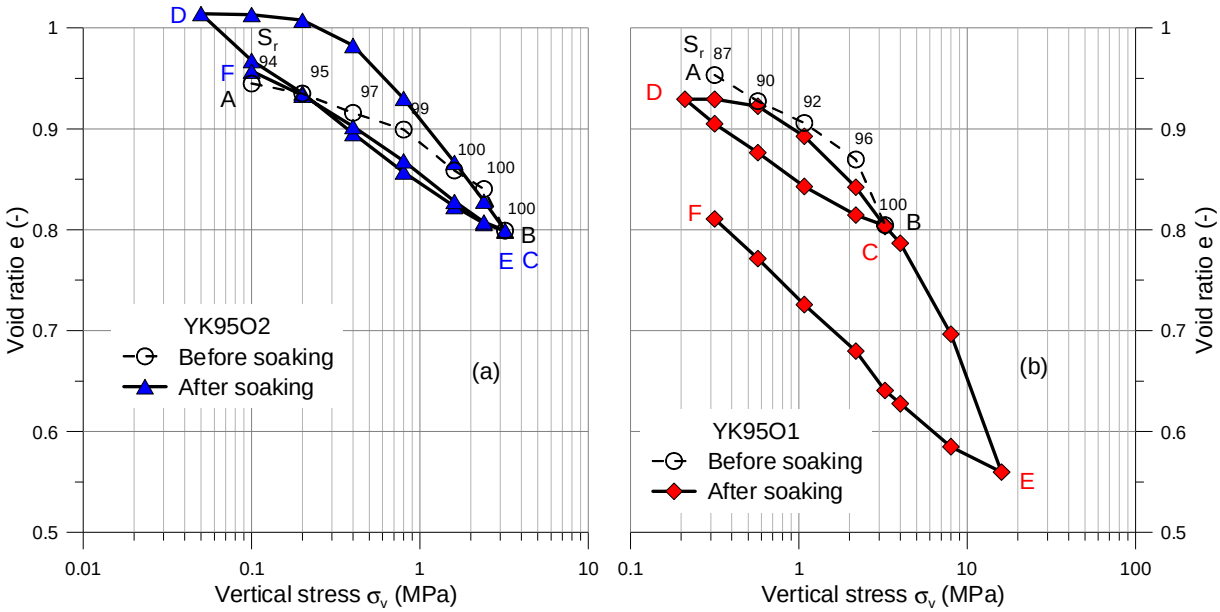
748
749 **Figure 10: Low- (a) and high- (b) pressure œdometer compression curves on YK64**

750



751
752 **Figure 11: Low- (a) and high- (b) pressure œdometer compression curves on YK73**

753



754
755 **Figure 12: Low- (a) and high- (b) pressure œdometer compression curves on YK95**

756

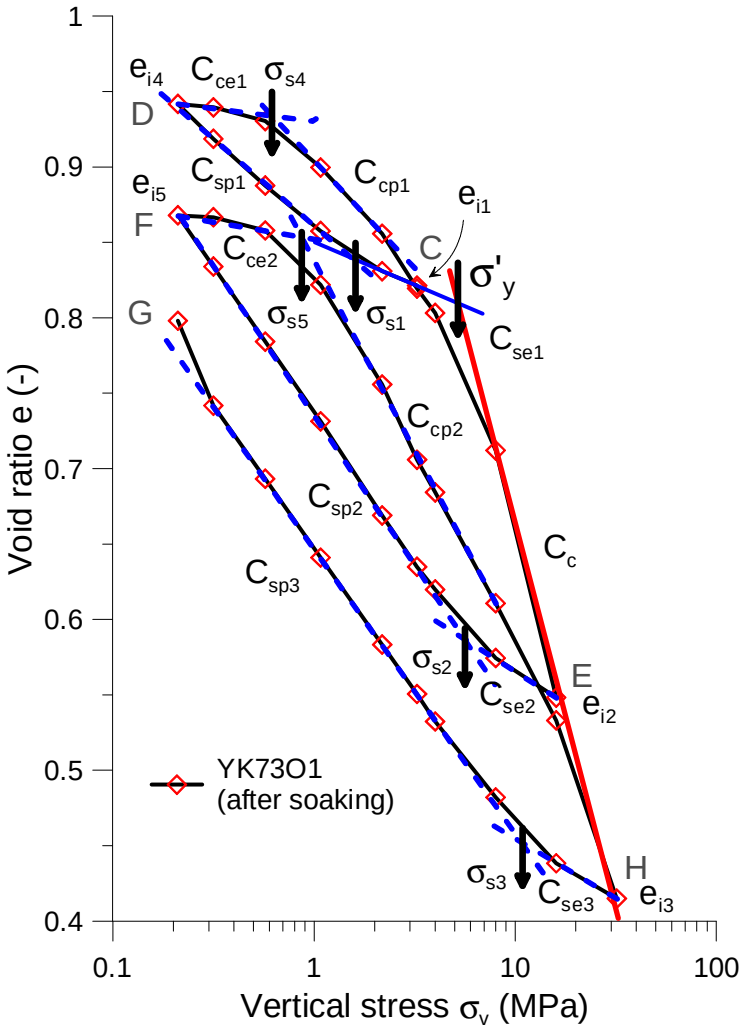
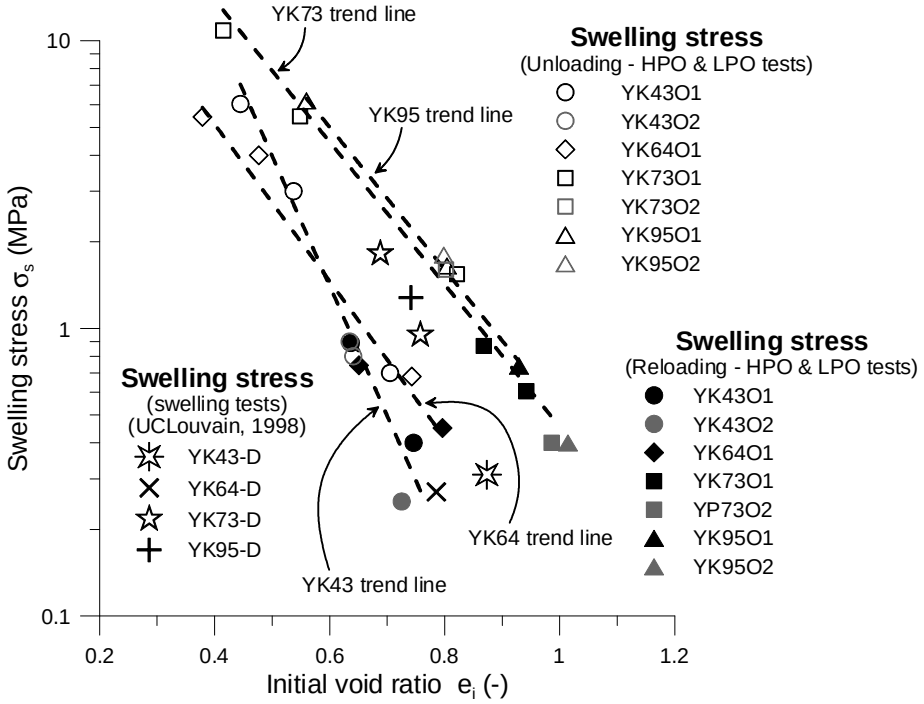
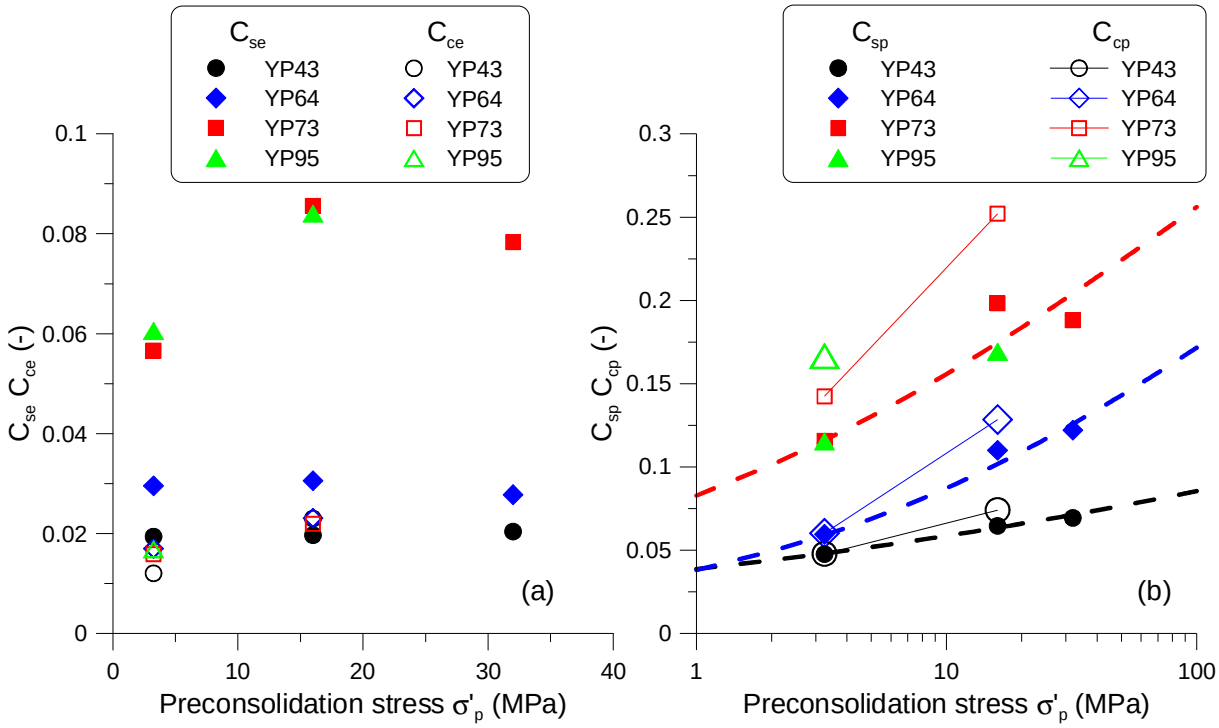


Figure 13: Parameter definitions



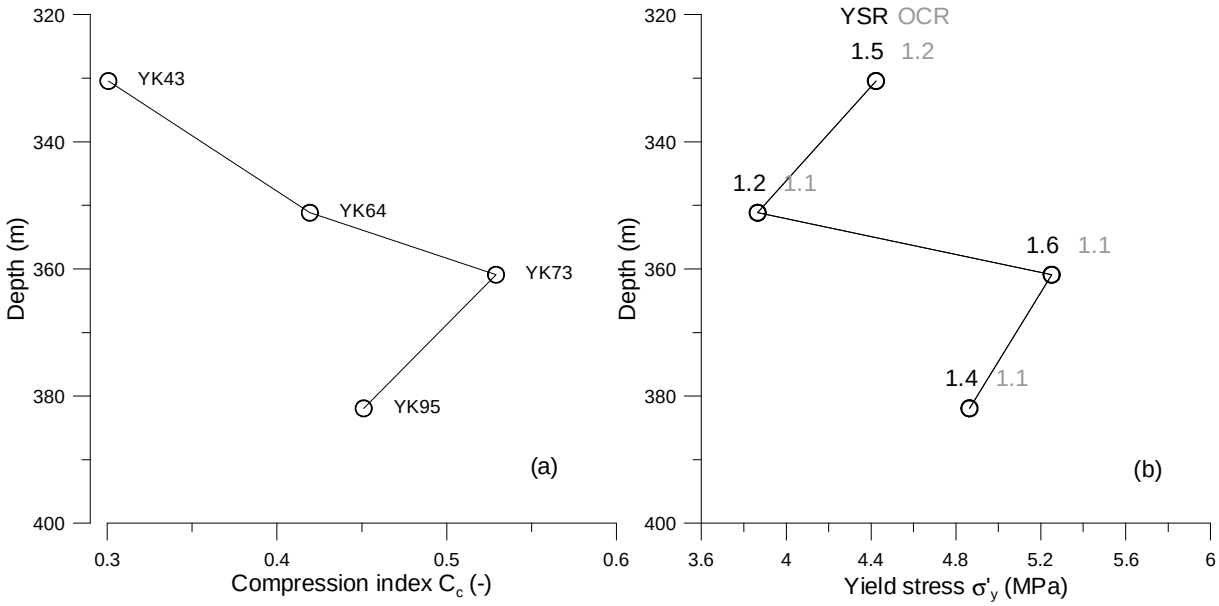
760
761
Figure 14: Swelling stress σ_s versus (initial) void ratio (e_i) e for Ypresian clay

762



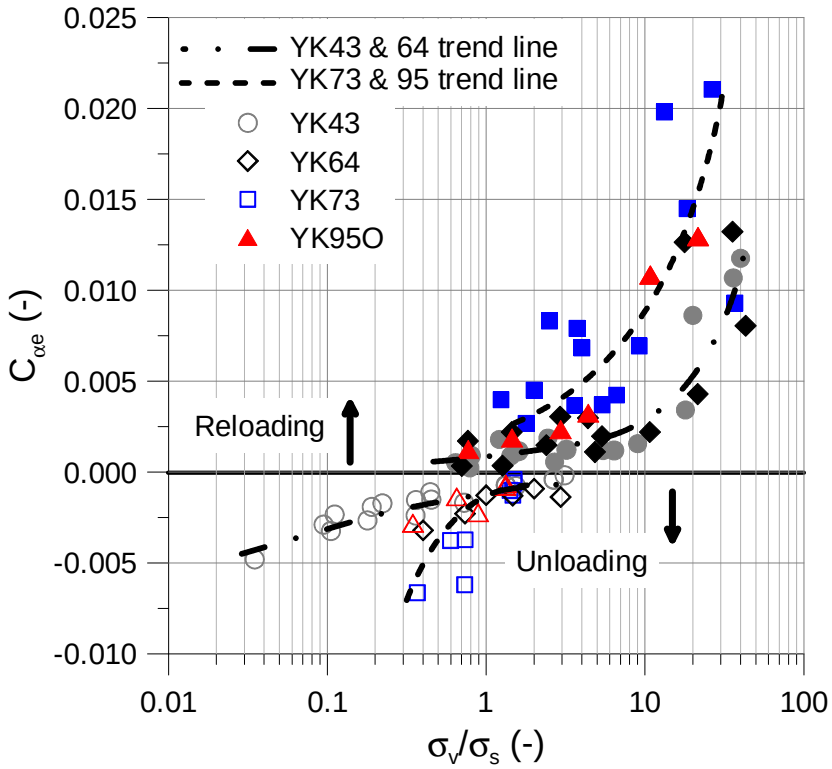
763
764
Figure 15: Variations of C_{se}, C_{ce} (a), C_{sp} and C_{cp} (b) versus preconsolidation stress σ'_p

765



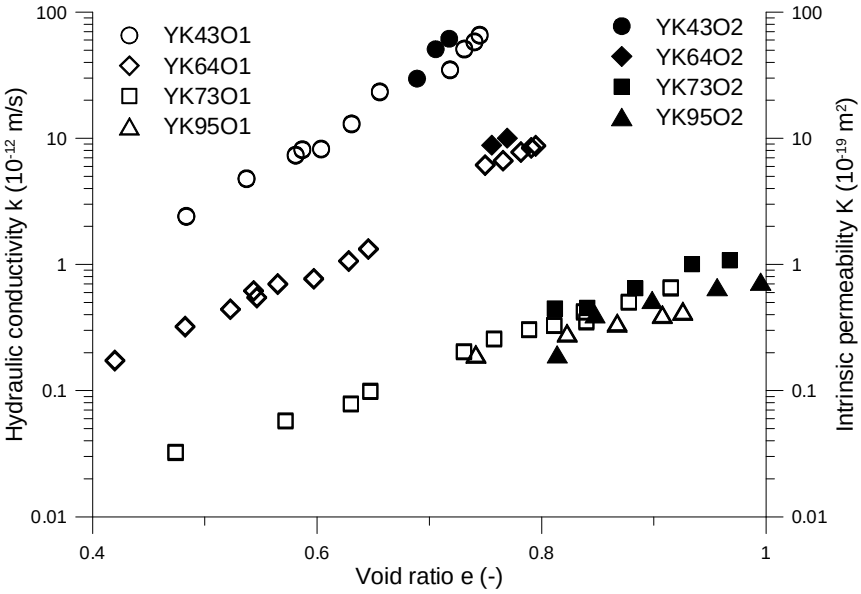
766
767 **Figure 16: Compression index C_c (a) and yield stress σ'_y (b) profiles**

768



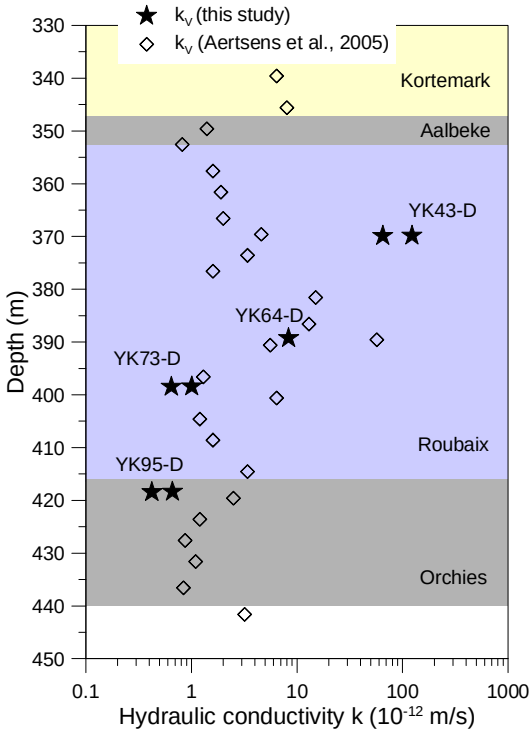
769
770 **Figure 17: Secondary compression/swelling coefficient**

771



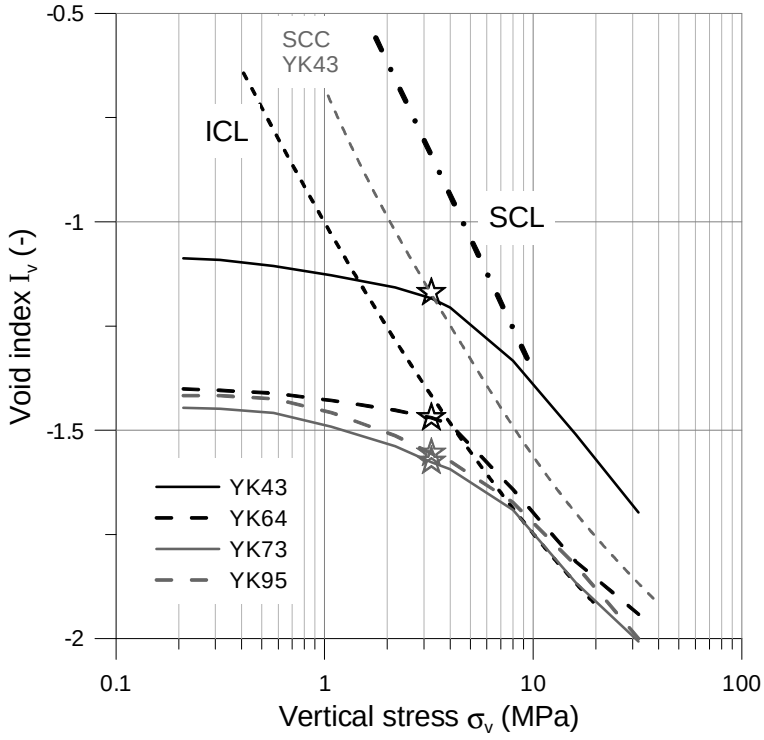
772
773 **Figure 18: Permeability of Ypresian clays**

774



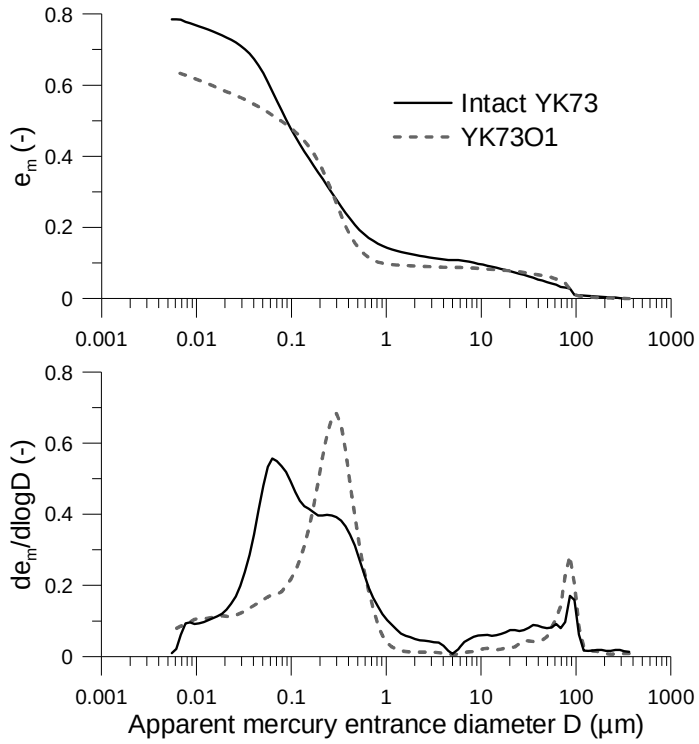
775
776 **Figure 19: Hydraulic conductivity profile for Ypresian clays at Doel (after Aertsons et al., 2005)**

777



778
779 **Figure 20: Normalized compression curves**

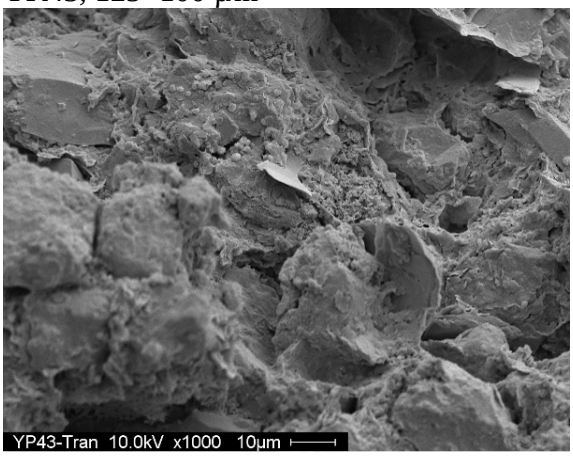
780



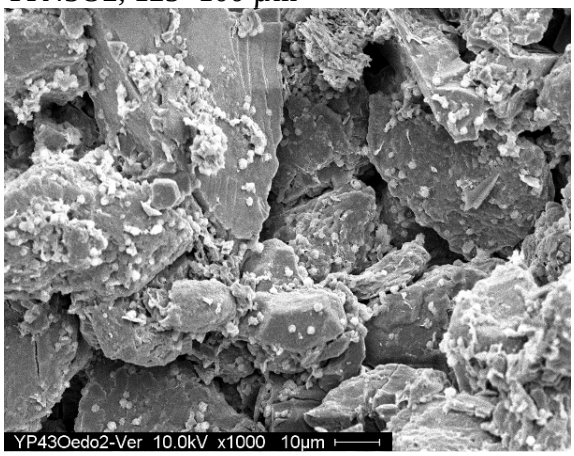
781
782 **Figure 21: Pore-size distribution curves of intact and after HPO test YK73**

783

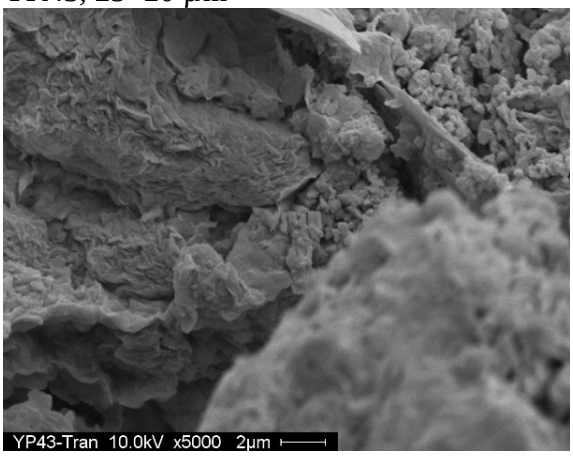
YK43, 125×100 µm



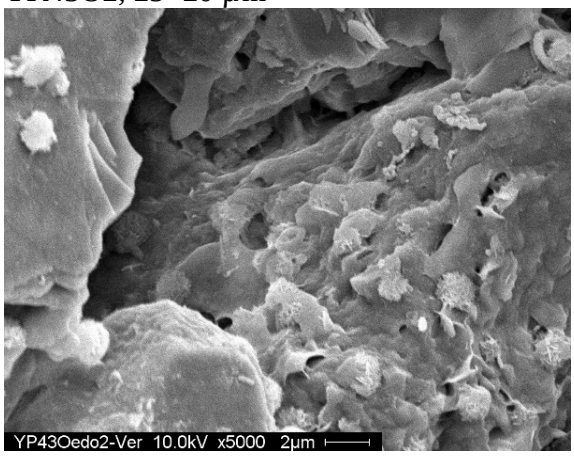
YK43O2, 125×100 µm



YK43, 25×20 µm



YK43O2, 25×20 µm



784 **Figure 22: SEM on intact (left) and after LPO test (right) YK43**

785

786